CHAPTER 19

ACOUSTOELASTICITY OF ELASTIC SOLIDS

K.Y. Kim and W. Sachse
Department of Theoretical and Applied Mechanics, Cornell University, Ithaca, New York, USA

Contents

19.1. INTRODUCTION

Acoustoelasticity is a branch of physical acoustics that deals with the variation of sound speed with elastic deformation and the relation between the wave speeds and the strength of materials in a stressed state. In this chapter we consider the acoustoelasticity of both bulk and surface acoustic waves in a homogeneously deformed elastic body and the determination of elastic stiffness coefficients from measurements of phase velocity of sound waves.

Properties of materials, including the strength of materials, change under stress. The changed strength reflects not only the internal strength change brought upon by the changes in internal structures, such as the change in interatomic and intermolecular distances, but also the stresses acting on the medium, whether the stresses are externally applied or internally locked. The internal change in strength can be described by using the thermodynamic elastic coefficients C_{ijkl}, and the overall strength change is described using the effective elastic coefficients K_{ijkl}. The strength change brought upon a material by the acting stresses varies linearly with those stresses. However, in general, the internal strength varies nonlinearly with stress, so do the effective elastic coefficients with stress. When a small-amplitude sound wave propagates through a stressed medium, the strain caused by the propagating wave must overcome a restoring force of both internal strength and acting stresses. Therefore, the density times the square of the

Handbook of Elastic Properties of Solids, Liquids, and Gases, edited by Levy, Bass, and Stern
Volume I: Dynamic Methods for Measuring the Elastic Properties of Solids

ISBN 0-12-445761-4 / $35.00

phase velocity of the sound wave represents the effective elastic coefficients, rather than the thermodynamic elastic coefficients it represents in a stress-free material.

The strengths of a material under adiabatic and isothermal processes are not equal. To account for the difference, the theory must be based on thermodynamic potentials, e.g., the internal and free energies, enthalpy, etc., rather than on a mechanical elastic energy density that ignores the entropy and temperature. Voigt [1] discussed the theory of thermoelasticity based on the thermodynamic potentials for the case of infinitesimal strains measured from the reference configuration of the stress-free natural state. For the case of finite deformation from the natural or the initially stressed state, his approach is quite inadequate, and it is better to use the thermodynamic potentials referred to the initially stressed state. Quite recently, Kim [2] described the theory of the thermoelasticity of an elastic solid in an initially stressed state in detail. In the thermodynamics of fluids, the stress acting on the fluids is isotropic (hydrostatic) pressure p, and its conjugate variable is volume V. Both p and V are scalar and can always be referred to the same current configuration under an arbitrary pressure. However, in a finitely deformed solid, the Cauchy stresses, corresponding to the hydrostatic pressure, are always represented using the current configuration, and representation of the strains requires a reference state that differs from the current configuration. Thus the strain and the Cauchy stress are not thermodynamic conjugate variables. With respect to a strain, it is necessary to define a thermodynamic conjugate variable, which refers to the same, initially stressed configuration to which the strain is referred. The conjugate thermodynamic variable is called the thermodynamic stress (second Piola–Kirchhoff stress), which is related to the Cauchy stress by the equation derived by Murnaghan [3]. The $(n-1)$'th $(n \geq 2)$ Lagrangian strain derivatives of the thermodynamic stress are called the n'th thermodynamic elastic coefficients, and the $(n-1)$'th $(n \geq 2)$ derivatives of the Cauchy stress with respect to the infinitesimal strain are called the effective elastic coefficients.

As already mentioned, the strength of a material under stress can be characterized by the second-order effective coefficients K_{ijkl}. Although in principle one can extend the definition to the third- and higher-order thermodynamic or effective coefficients in an initially stressed state, their utility is of limited value, except for the third- and higher-order thermodynamic constants defined at zero stress. Here, instead of defining third- and higher-order elastic coefficients in the initial state, we relate K_{ijkl} coefficients defined in the initial state both to the second-order elastic constants (SOEC), third-order elastic constants (TOEC), and higher-order elastic constants (HOEC), all defined in the natural state, and to the initial strains referred to the natural state, as long as the deformation from the natural state to the initial state is a smoothly varying elastic process. However, this chapter does not intend to tabulate these relations for all kinds of symmetry groups and crystal classes. For rubberlike polymer materials and in the vicinity of a phase transformation or the critical phenomenon of ordinary solids, this relation using the SOEC and HOEC is no longer valid. However, one can still study the strength of rubberlike polymers and the phase transformation of ordinary materials by investigating the behavior of K_{ijkl} versus stress for the former materials and the behavior of K_{ijkl} across phase transformation stress for the latter materials.

From the atomic point of view, especially in the language of lattice dynamics, TOEC and HOEC represent anharmonic effects of solids. Since the elastic waves are in leading harmonic approximation, the same as the long-wavelength acoustic phonons, K_{ijkl}, TOEC and HOEC are related to the phonon frequency distribution versus strain, phonon lifetimes, thermal expansion, thermal conductivity, etc. The atomic theory of the strength of solids lies outside the scope of this chapter. Interested readers are referred to [4, 5, 6]. Acoustoplasticity, which deals with the relations between sound speed and plastic deformation, is also outside the scope of this chapter, which is solely

devoted to elastic deformation. This chapter is centered around the phenomenological relations between K_{ijkl} and the stresses exerted on a medium, the determination of K_{ijkl} from the measured phase velocities, and the possible determination of applied or residual stresses from the observed phase velocities of bulk and surface acoustic waves.

19.2. THERMODYNAMIC AND EFFECTIVE ELASTIC COEFFICIENTS

Consider a prestressed elastic body that has undergone an arbitrary homogeneous deformation $\mathbf{U}^I$ from the stress-free natural state. The Cartesian coordinates of a particle in the natural state are denoted by vector $\mathbf{a}$. The prestressed body is said to be in an initial state, which is a static state denoted by the Cartesian coordinates $\mathbf{X}$. The initial state can be any state, which can include the natural state, since $\mathbf{U}^I$ is arbitrary. Finally, a small deformation $\mathbf{u}$ is superposed on the initial state. We call this state a current or present state and denote its Cartesian coordinates by $\mathbf{x}$. We denote the density of the natural, initial, and current states by ρ_a, ρ_X, and ρ_x, respectively, and the Cauchy stresses in the corresponding states by $\sigma_{ij}(\mathbf{a})$, $\sigma_{ij}(\mathbf{X})$, and $\sigma_{ij}(\mathbf{x})$, respectively. Deformations $\mathbf{u}$, $\mathbf{U}$, and $\mathbf{U}^I$ are expressed as

$$\mathbf{u} = \mathbf{x} - \mathbf{X} \quad \mathbf{U} = \mathbf{x} - \mathbf{a} \quad \mathbf{U}^I = \mathbf{X} - \mathbf{a} \tag{19.1}$$

Let a tensor $\mathbf{T}(\mathbf{A};\mathbf{B})$ denote a physical variable, which is evaluated in the state represented by a coordinate system $\mathbf{A}$ and which takes $\mathbf{B}$ as a reference coordinate system from which a deformation is measured. Both $\mathbf{A}$ and $\mathbf{B}$ can be $\mathbf{x}$, $\mathbf{X}$, or $\mathbf{a}$. When both $\mathbf{A}$ and $\mathbf{B}$ are represented by the same coordinate system, we denote the tensor $\mathbf{T}$ by a single argument, as shown in the examples $\mathbf{T}(\mathbf{a};\mathbf{a}) = \mathbf{T}(\mathbf{a})$, $\mathbf{T}(\mathbf{X};\mathbf{X}) = \mathbf{T}(\mathbf{X})$, and $\mathbf{T}(\mathbf{x};\mathbf{x}) = \mathbf{T}(\mathbf{x})$. The Cauchy stresses $\sigma_{ij}(\mathbf{a})$, $\sigma_{ij}(\mathbf{X})$, and $\sigma_{ij}(\mathbf{x})$ are the typical examples of this representation and are always evaluated at and referred for deformation to the same coordinate system.

The Lagrangian strains $\zeta_{ij}(\mathbf{x};\mathbf{X})$ and $\varepsilon_{ij}(\mathbf{x};\mathbf{X})$, both evaluated in the current state $\mathbf{x}$ and referred for deformation to the initially stressed state $\mathbf{X}$, are given by

$$\zeta_{ij}(\mathbf{x};\mathbf{X}) = \frac{1}{2}\left(\frac{\partial x_m}{\partial X_i}\frac{\partial x_m}{\partial X_j} - \delta_{ij}\right) = \frac{1}{2}\left(\frac{\partial u_i}{\partial X_j} + \frac{\partial u_j}{\partial X_i} + \frac{\partial u_k}{\partial X_i}\frac{\partial u_k}{\partial X_j}\right)$$

$$= \varepsilon_{ij} + \frac{1}{2}\frac{\partial u_k}{\partial X_i}\frac{\partial u_k}{\partial X_j} \tag{19.2}$$

$$\varepsilon_{ij}(\mathbf{x};\mathbf{X}) = (\partial u_i/\partial X_j + \partial u_j/\partial X_i)/2 \tag{19.3}$$

The Lagrangian strains $\zeta_{ij}(\mathbf{X};\mathbf{a})$ and the infinitesimal strains $\varepsilon_{ij}(\mathbf{X};\mathbf{a})$ are obtained by replacing in Eqs. 19.2 and 19.3 $\mathbf{x}$, $\mathbf{X}$, and $\mathbf{u}$ by $\mathbf{X}$, $\mathbf{a}$, and $\mathbf{U}^I$, respectively. In Eq. 19.2 and henceforth, it is understood that the Einstein's convention on the summation over the repeated indices is implied, unless otherwise specified.

With reference to the initial state, we define according to Brugger's convention [7] the thermodynamic stress $\tau_{ij}(\mathbf{x};\mathbf{X})$ and the adiabatic and isothermal thermodynamic elastic stiffness/compliance coefficients C_{ijkl} and S_{ijkl} of the n'th ($n \geq 2$) order as

$$\tau_{ij}(\mathbf{x};\mathbf{X}) \equiv \rho_x\left(\frac{\partial U}{\partial \zeta_{ij}}\right)_{S;\mathbf{x}} = \rho_X\left(\frac{\partial F}{\partial \zeta_{ij}}\right)_{T;\mathbf{x}} \tag{19.4}$$

$$C^S_{ijkl\ldots}(\mathbf{x};\mathbf{X}) \equiv \rho_X(\partial^n U/\partial\zeta_{ij}\partial\zeta_{kl}\ldots)_{S;\mathbf{x}} = (\partial\tau^{n-1}_{ij}/\partial\zeta_{kl}\ldots)_{S;\mathbf{x}} \quad (n \geq 2) \tag{19.5}$$

$$C^T_{ijkl\ldots}(\mathbf{x};\mathbf{X}) \equiv \rho_X(\partial^n F/\partial\zeta_{ij}\partial\zeta_{kl}\ldots)_{T;\mathbf{x}} = (\partial\tau^{n-1}_{ij}/\partial\zeta_{kl}\ldots)_{T;\mathbf{x}} \quad (n \geq 2) \tag{19.6}$$

$$S^S_{ijkl\ldots}(\mathbf{x};\mathbf{X}) \equiv -\rho_X(\partial^n H/\partial\tau_{ij}\partial\tau_{kl}\ldots)_{S;\mathbf{x}} = (\partial\zeta^{n-1}_{ij}/\partial\tau_{kl}\ldots)_{S;\mathbf{x}} \quad (n \geq 2) \tag{19.7}$$

$$S^T_{ijkl\ldots}(\mathbf{x};\mathbf{X}) \equiv -\rho_X(\partial^n G/\partial\tau_{ij}\partial\tau_{kl}\ldots)_{T;\mathbf{x}} = (\partial\zeta^{n-1}_{ij}/\partial\tau_{kl}\ldots)_{T;\mathbf{x}} \quad (n \geq 2) \tag{19.8}$$

where U, F, H, and G are, respectively, the internal energy, Helmholtz free energy, enthalpy, and Gibbs free energy per unit mass. S denotes the entropy and T the temperature. Both $C^{T \text{ or } S}_{ijkl\ldots}$ and $S^{T \text{ or } S}_{ijkl\ldots}$ coefficients are generally a function of stress. In the special case of the initial state being identical to the stress-free natural state $\mathbf{a}$, the quantities given in Eqs. 19.4–19.8 are defined by replacing $\mathbf{X}$ by $\mathbf{a}$.

The special types of thermodynamic elastic stiffness coefficients are the SOEC and the TOEC defined as

$$C^{S \text{ or } T}_{ijkl}(\mathbf{a}) = C^{S \text{ or } T}_{ijkl}(\mathbf{a};\mathbf{a}) \quad S^{S \text{ or } T}_{ijkl}(\mathbf{a}) = S^{S \text{ or } T}_{ijkl}(\mathbf{a};\mathbf{a}) \quad \text{(SOEC)} \tag{19.9}$$

$$C^{S \text{ or } T}_{ijklmn}(\mathbf{a}) = C^{S \text{ or } T}_{ijklmn}(\mathbf{a};\mathbf{a}) \quad S^{S \text{ or } T}_{ijklmn}(\mathbf{a}) = S^{S \text{ or } T}_{ijklmn}(\mathbf{a};\mathbf{a}) \quad \text{(TOEC)} \tag{19.10}$$

which are all evaluated at and referred to the stress-free natural coordinate $\mathbf{a}$. When the superscript S or T is omitted in the notation of the elastic stiffness and compliance coefficients, it is understood that they refer to both adiabatic and isothermal processes. The SOEC satisfy the full symmetry relations in their subscript indices and can be abbreviated using the Voigt notations. The SOEC matrices $[C_{\alpha\beta}(\mathbf{a})]$ and $[S_{\alpha\beta}(\mathbf{a})](\alpha, \beta = 1, 2, \ldots 6)$ are symmetric, i.e., $C_{\alpha\beta} = C_{\beta\alpha}$ and $S_{\alpha\beta} = S_{\beta\alpha}$, and have in general 21 independent elements. They satisfy the reciprocal relation $S_{\alpha\beta}C_{\beta\lambda} = \delta_{\alpha\lambda}$, where δ denotes the Kronecker delta. Differentiating this reciprocal relation with respect to Lagrangian strain $\zeta_\mu(\mathbf{x};\mathbf{a})$ yields

$$S_{\alpha\beta\gamma}(\mathbf{a}) = -S_{\alpha\lambda}(\mathbf{a})S_{\beta\mu}(\mathbf{a})S_{\gamma\nu}(\mathbf{a})C_{\lambda\mu\nu}(\mathbf{a}) \tag{19.11}$$

$$C_{\alpha\beta\gamma}(\mathbf{a}) = -C_{\alpha\lambda}(\mathbf{a})C_{\beta\mu}(\mathbf{a})C_{\gamma\nu}(\mathbf{a})S_{\lambda\mu\nu}(\mathbf{a}) \tag{19.12}$$

Equations 19.11 and 19.12 indicate that one can determine the set of the compliance SOEC and TOEC from knowledge of the set of the stiffness SOEC and TOEC, and vice versa. Both TOEC $C_{\alpha\beta\gamma}(\mathbf{a})$ and $S_{\alpha\beta\gamma}(\mathbf{a})$ sets have in general 56 independent elements.

Equation 19.4 indicates that the thermodynamic stress depends on the choice of the reference coordinate system for deformation. For example, $\tau_{ij}(\mathbf{x};\mathbf{X})$ is related to $\tau_{kl}(\mathbf{x};\mathbf{a})$ through a coordinate transformation by

$$\tau_{ij}(\mathbf{x};\mathbf{X}) = \frac{\rho_X}{\rho_a}\frac{\partial X_i}{\partial a_k}\frac{\partial X_j}{\partial a_l}\tau_{kl}(\mathbf{x};\mathbf{a}) \tag{19.13}$$

Similarly, one obtains

$$C_{ijkl}(\mathbf{X}) = C_{ijkl}(\mathbf{X};\mathbf{X}) = \frac{\rho_X}{\rho_a}\frac{\partial X_i}{\partial a_m}\frac{\partial X_j}{\partial a_n}\frac{\partial X_k}{\partial a_p}\frac{\partial X_l}{\partial a_q}C_{mnpq}(\mathbf{X};\mathbf{a}) \tag{19.14}$$

which can be expressed via Eqs. 19.5, 19.6, 19.9, and 19.10 in terms of the SOEC and TOEC as

$$C_{ijkl}(\mathbf{X}) = \frac{\rho_X}{\rho_a}\frac{\partial X_i}{\partial a_m}\frac{\partial X_j}{\partial a_n}\frac{\partial X_k}{\partial a_p}\frac{\partial X_l}{\partial a_q}[C_{mnpq}(\mathbf{a}) + C_{mnpqrs}(\mathbf{a})\zeta_{rs}(\mathbf{X};\mathbf{a}) + \ldots] \tag{19.15}$$

A Cauchy stress $\sigma_{ij}(\mathbf{X})$ is equal to the thermodynamic stress $\tau_{ij}(\mathbf{X}) = \tau_{ij}(\mathbf{X};\mathbf{X})$ and is related to the thermodynamic stresses $\tau_{kl}(\mathbf{X};\mathbf{a})$ via Eq. 19.13 by Murnaghan's relation [3]

$$\sigma_{ij}(\mathbf{X}) = \tau_{ij}(\mathbf{X}) = \tau_{ij}(\mathbf{X};\mathbf{X}) = \frac{\rho_X}{\rho_a}\frac{\partial X_i}{\partial a_k}\frac{\partial X_j}{\partial a_l}\tau_{kl}(\mathbf{X};\mathbf{a}) \tag{19.16}$$

It follows from Eqs. 19.4–19.10 that $\sigma_{ij}(\mathbf{X})$ can be written in terms as the SOEC and TOEC as

$$\sigma_{ij}(\mathbf{X}) = \frac{\rho_X}{\rho_a}\frac{\partial X_i}{\partial a_k}\frac{\partial X_j}{\partial a_l}\left[C_{klmn}(\mathbf{a})\zeta_{mn}(\mathbf{X};\mathbf{a}) + \frac{1}{2}C_{klmnpq}(\mathbf{a})\zeta_{mn}(\mathbf{X};\mathbf{a})\zeta_{pq}(\mathbf{X};\mathbf{a}) + \ldots\right] \tag{19.17}$$

We also define in the initial state $\mathbf{X}$ the effective elastic stiffnesses K_{ijkl} and the effective elastic compliances Q_{ijkl} of the second order, which indicate the measure of material strength in the initial state, as [8]

$$K_{ijkl}(\mathbf{X}) = (\partial\sigma_{ij}/\partial\varepsilon_{kl})_{\mathbf{X}} = C_{ijkl}(\mathbf{X}) - \sigma_{ij}(\mathbf{X})\delta_{kl} + (1/2)[\sigma_{ik}(\mathbf{X})\delta_{jl} + \sigma_{il}(\mathbf{X})\delta_{jk} + \sigma_{jk}(\mathbf{X})\delta_{il} + \sigma_{jl}(\mathbf{X})\delta_{ik}] \tag{19.18}$$

$$Q_{ijkl}(\mathbf{X}) = (\partial\varepsilon_{ij}/\partial\sigma_{kl})_{\mathbf{X}} \tag{19.19}$$

where δ denotes a Kronecker delta. It is noted that while the full symmetry relations $C_{ijkl} = C_{jikl} = C_{ijlk} = C_{klij}$ in the thermodynamic elastic stiffness coefficients defined in Eqs. 19.5 and 19.6 are maintained, the full symmetry is lost in the effective elastic coefficients K_{ijkl} and Q_{ijkl}, unless the stress acting on the specimen is hydrostatic, i.e., $\sigma_{ij} = s\delta_{ij}$, where s is a positive or negative scalar variable. K_{ijkl} obey the relations $K_{ijkl} = K_{jikl} = K_{ijlk}$ along with

$$K_{ijkl} - K_{klij} = \delta_{ij}\sigma_{kl} - \delta_{kl}\sigma_{ij} \tag{19.20}$$

K_{ijkl} and Q_{ijkl} satisfy the reciprocal relation $K_{\alpha\gamma}Q_{\gamma\beta} = \delta_{\alpha\beta}$ or $[Q_{\alpha\beta}] = [K_{\alpha\beta}]^{-1}$, where α and β are abbreviated Voigt notations ($\alpha, \beta = 1, 2, \ldots, 6$).

It is readily shown from Eq. 19.18 that

$$[K_{\alpha\beta}] = \begin{bmatrix} C_{11}+\sigma_1 & C_{12}-\sigma_1 & C_{13}-\sigma_1 & C_{14} & C_{15}+\sigma_5 & C_{16}+\sigma_6 \\ C_{12}-\sigma_2 & C_{22}+\sigma_2 & C_{23}-\sigma_2 & C_{24}+\sigma_4 & C_{25} & C_{26}+\sigma_6 \\ C_{13}-\sigma_3 & C_{23}-\sigma_3 & C_{33}+\sigma_3 & C_{34}+\sigma_4 & C_{35}+\sigma_5 & C_{36} \\ C_{14}-\sigma_4 & C_{24} & C_{34} & C_{44}+(\sigma_2+\sigma_3)/2 & C_{45}+\sigma_6/2 & C_{46}+\sigma_5/2 \\ C_{15} & C_{25}-\sigma_5 & C_{35} & C_{45}+\sigma_6/2 & C_{55}+(\sigma_1+\sigma_3)/2 & C_{56}+\sigma_4/2 \\ C_{16} & C_{26} & C_{36}-\sigma_6 & C_{46}+\sigma_5/2 & C_{56}+\sigma_4/2 & C_{66}+(\sigma_1+\sigma_2)/2 \end{bmatrix} \tag{19.21}$$

where all the $K_{\alpha\beta}$ elements are evaluated in the initial state $\mathbf{X}$.

The *in situ* isothermal material strengths $K^T_{\alpha\beta}$ and $Q^T_{\alpha\beta}$ in an arbitrarily stressed initial state can be obtained by very slow, static tension, compression, and torsion tests. It will be shown in the following that elastic moduli obtained from ultrasonic phase velocity measurements are not $C^S_{\alpha\beta}$ but adiabatic effective elastic stiffness moduli $K^S_{\alpha\beta}$. The literature is arbitrary about the choice and definition of the effective elastic coefficient. We choose K_{ijkl}, defined by Eq. 19.18, as the effective elastic coefficients. There are several reasons behind our choice: first, K_{ijkl} represent the strength of a medium in a stressed state; second, K_{ijkl} reduce to the SOEC C_{ijkl} (**a**) in the special case of the stress-free state; third, the density times the square of phase velocity measured in a stressed state is equal to a K_{ijkl} element or a combination of K_{ijkl} elements, as will be shown; fourth, K_{ijkl} are compatible with the definition of the effective elastic constants originally introduced by Birch [9]; and finally, K_{ijkl} fit consistently into the general context of the thermodynamics of an elastic solid [2].

It is advantageous for the study of the wave propagation in a stressed state to define in an initially stressed state $\mathbf{X}$ the isentropic elastic stiffness coefficients $B^S_{ijkl}(\mathbf{X}) = B^S_{ijkl}(\mathbf{X};\mathbf{X})$ and $A^S_{ijkl}(\mathbf{X};\mathbf{a})$ as [8,10,11]

$$B^S_{ijkl}(\mathbf{X}) \equiv \left(\frac{\rho_X\partial^2 U}{\partial(\partial x_k/\partial X_l)\partial(\partial x_i/\partial X_j)}\right)_{S;\mathbf{X}} = \delta_{ik}\sigma_{jl}(\mathbf{X}) + C^S_{ijkl}(\mathbf{X}) \tag{19.22}$$

$$A^S_{ijkl}(\mathbf{X};\mathbf{a}) \equiv \left(\frac{\rho_a \partial^2 U}{\partial(\partial x_k/\partial a_l)\partial(\partial x_i/\partial a_j)}\right)_{S;\mathbf{X}}$$

$$= \delta_{ik}\tau_{jl}(\mathbf{X};\mathbf{a}) + \frac{\partial X_i}{\partial a_p}\frac{\partial X_k}{\partial a_q}C^S_{pjql}(\mathbf{X};\mathbf{a}) \tag{19.23}$$

19.3. EQUATION OF MOTION IN AN INITIALLY STRESSED STATE

Using $B^S_{ijkl}(\mathbf{X})$ in Eq. 19.22 and $A^S_{ijkl}(\mathbf{X};\mathbf{a})$ in Eq. 19.23, the linearlized equations of motion about the initially stressed state can be written as [8,10,11]

$$\rho_X \ddot{x}_i = B^S_{ijkl}(\mathbf{X})\frac{\partial^2 x_k}{\partial X_j \partial X_l} \tag{19.24}$$

$$\rho_a \ddot{x}_i = A^S_{ijkl}(\mathbf{X};\mathbf{a})\frac{\partial^2 x_k}{\partial a_j \partial a_l} \tag{19.25}$$

By seeking small-amplitude plane wave solutions for Eq. 19.24 in the form of

$$x_i - X_i = u_i \exp[i\omega(t - n_s X_s/V)] \tag{19.26}$$

one obtains

$$[B^S_{ijkl}(\mathbf{X})n_j n_l - \rho_X V^2 \delta_{ik}]u_k = \left[C^S_{ijkl}(\mathbf{X})n_j n_l - \{\rho_X V^2 - \sigma_{jl}(\mathbf{X})n_j n_l\}\delta_{ik}\right] u_k = 0 \tag{19.27}$$

Similarly, assuming the solutions for Eq. 19.25 in the form of

$$x_i - X_l = u_i \exp[i\omega(t - m_s a_s/W)] \tag{19.28}$$

yields

$$[A^S_{ijkl}(\mathbf{X};\mathbf{a})m_j m_l - \rho_a W^2 \delta_{ik}]u_k = 0 \tag{19.29}$$

In Eqs. 19.26–19.29, $\mathbf{n}$ and V denote the actual direction and phase velocity of wave propagation in an initially stressed $\mathbf{X}$, respectively, and $\mathbf{m}$ and W are the corresponding direction and velocity in the natural configuration $\mathbf{a}$. Denoting a transit time of the plane wave and its acoustic path length in the initial state $\mathbf{X}$ by τ and L_X, respectively, and the corresponding acoustic path length in the natural configuration by L_a, it follows that $V = L_X/\tau$ and $W = L_a/\tau$. Thurston and Brugger [11] call W the *natural velocity*.

In the special case of the initial state $\mathbf{X}$ being identical to the stress-free natural state, both Eq. 19.27 and Eq. 19.29 reduce to the Christoffel equation

$$[C_{ijkl}(\mathbf{a})m_j m_l - \rho_a V^2 \delta_{ik}]U_k = 0 \tag{19.30}$$

where $C_{ijkl}(\mathbf{a})m_j m_i$ is called the Christoffel tensor with an eigenvalue $\rho_a V^2$ and an eigenvector U_k.

Eq. 19.27, derived in the initial state $\mathbf{X}$, can be interpreted either as having an effective Christoffel tensor $B_{ijkl}(\mathbf{X})n_j n_l$ associated with an eigenvalue $\rho_X V^2$ or as having an effective Christoffel tensor $C_{ijkl}(\mathbf{X})n_j n_l$ associated with an eigenvalue $\rho_X V^2 - \sigma_{jl}(\mathbf{X})n_j n_l$. As shown in Section 19.5, the latter interpretation is particularly useful in checking out the solution of surface acoustic wave (SAW) propagation on the surface of a prestressed elastic body.

Toupin and Bernstein [10] transformed Eq. 19.29 into a representation that depends only on the strain from the natural state $\mathbf{a}$, independent of rotation from $\mathbf{a}$, by transforming $\mathbf{u}$ via $u_k = (\partial X_k/\partial a_p)U_p$. Thurston and Brugger [11] made use of the transformed representation for the determination of the TOEC, since one can see from

Eqs. 19.29, 19.23, 19.5, 19.9, and 19.10 that pressure, stress, or strain derivatives of $\rho_a W^2$ taken in the stress-free natural state are expressed in terms of the SOEC and TOEC. The method of Thurston and Brugger has the advantage that, given the acoustic path length L_a in the stress-free state, it requires only the measurement of ultrasonic transit times τ for a stressed specimen, obviating the need to measure actual acoustic path lengths L_X. Further details using Eq. 19.29 on the TOEC are provided by Wallace [12] and in Chapter 21 by Breazeale. An early determination of a complete set of three TOEC for some isotropic materials in the natural stress-free state was achieved by Hughes and Kelley [13] from the measured dependence of bulk wave speeds on uniaxial stress, using Murnaghan's theory of finite deformation [3], and a complete set of six TOEC for a cubic crystal was first measured by Bateman *et al.* [14], using a germanium crystal as a specimen and formulas developed by Seeger and Buck [15]. Since then, there have been numerous publications on the TOEC of a variety of materials, and they are compiled by Every and McCurdy [16].

Useful as the concept of natural velocity W and $\rho_a W^2$ for determination of the TOEC is, neither W nor $\rho_a W^2$ is an actual physical quantity. For an investigation of the *in situ* strength of materials, phase transitions, equations of state of solids, surface acoustic waves (SAWs), residual stresses of structures, etc., under general stresses, it is useful to look at the behavior of the effective elastic coefficients $K_{ijkl}(\mathbf{X})$ defined in Eq. 19.18, as these coefficients are generally nonlinear functions of stress and behave even anomalously in the vicinity of phase transition stress [17]. In the next sections we will discuss a determination of $K_{ijkl}(\mathbf{X})$ using bulk waves and the propagation of SAWs in the initial state $\mathbf{X}$.

19.4. DETERMINATION OF EFFECTIVE ELASTIC COEFFICIENTS USING BULK WAVES

19.4.1. General Formulation Using the Wave Propagation Coefficients

The effective elastic coefficients $K_{ijkl}(\mathbf{X})$ defined in Eq. 19.18 can be obtained from $B^S_{ijkl}(\mathbf{X})$ coefficients, which are determined via measurements of phase velocities V of bulk waves of either the longitudinal or transverse mode using Eq. 19.27. However, the $B^S_{ijkl}(\mathbf{X})$ coefficients in Eq. 19.22 lack the full symmetry found in the C_{ijkl} coefficients shown in Eq. 19.15 and cannot be abbreviated using the Voigt notation. Following Huang [4,18], we introduce a new set of elastic stiffness coefficients $C\tilde{C}_{ijkl}$ called the wave propagation coefficients, which are defined as

$$\tilde{C}_{ijkl}(\mathbf{X}) = [B^S_{ikjl}(\mathbf{X}) + B^S_{il\,jk}(\mathbf{X})]/2 = \delta_{ij}\sigma_{kl}(\mathbf{X}) + [C^S_{ikjl}(\mathbf{X}) + C^S_{il\,jk}(\mathbf{X})]/2 \quad (19.31)$$

Using the $\tilde{C}_{ijkl}$ coefficients, the equation of motion in Eq. 19.24 becomes

$$\rho_X \ddot{u}_i = \tilde{C}_{ijkl}(\mathbf{X}) \frac{\partial^2 u_j}{\partial X_k \partial X_l} \quad (19.32)$$

Note that $\tilde{C}_{ijkl} = \tilde{C}_{jikl}$ and $\tilde{C}_{ijkl} = \tilde{C}_{ijlk}$. $\tilde{C}_{ijkl}$ coefficients obey the Huang's conditions

$$\tilde{C}_{ijkl} - \tilde{C}_{klij} = \tilde{C}_{\alpha\beta} - \tilde{C}_{\beta\alpha} = \delta_{ij}\sigma_{kl} - \delta_{kl}\sigma_{ij} \quad (19.33)$$

where the subscripts α and β ($\alpha,\beta = 1, 2 \ldots 6$) are the Voigt indices. When the stresses acting on the medium are hydrostatic or zero, Huang's conditions become zero and then the wave propagation coefficients $\tilde{C}_{ijkl}$ possess the full symmetry relations as found in the C_{ijkl} coefficients. Solving Eq. 19.32 with the plane waves described in

Eq. 19.26 yields

$$(\tilde{C}_{ijkl} n_k n_l - \rho_X V^2 \delta_{ij}) u_j = 0 \tag{19.34}$$

$$\det|\Gamma_{ij} - \rho_X V^2 \delta_{ij}| = 0 \tag{19.35}$$

where $\Gamma_{ij}(\mathbf{n}) = \tilde{C}_{ijkl} n_k n_l$ is the symmetric acoustical tensor whose eigenvectors are the possible directions of particle displacement and whose eigenvalues are the corresponding values of $\rho_X V^2$. In terms of abbreviated Voigt notations α and β, Γ_{ij} is written as $\Gamma_{ij} = \Gamma_\alpha = \tilde{C}_{\alpha\beta} N_\beta$, where $N_1 = n_1^2$, $N_2 = n_2^2$, $N_3 = n_3^2$, $N_4 = 2n_2 n_3$, $N_5 = 2n_1 n_3$, and $N_6 = 2n_1 n_2$.

Both $\tilde{C}_{ijkl}$ and K_{ijkl} coefficients obey the same symmetry relations and the same Huang's conditions, as shown in Eqs. 19.33 and 19.20. Huang's conditions impose 10 independent constraints on the $[\tilde{C}_{\alpha\beta}]$ and $[K_{\alpha\beta}]$ coefficients. Therefore, both 6×6 arrays $[\tilde{C}_{\alpha\beta}]$ and $[K_{\alpha\beta}]$ have the maximum of 26 independent elements. It is readily shown from Eq. 19.31 that the 6×6 array $[\tilde{C}_{\alpha\beta}]$ can be written as

$$[\tilde{C}_{\alpha\beta}] = \begin{bmatrix} C_{11}+\sigma_1 & C_{66}+\sigma_2 & C_{55}+\sigma_3 & C_{56}+\sigma_4 & C_{15}+\sigma_5 & C_{16}+\sigma_6 \\ C_{66}+\sigma_1 & C_{22}+\sigma_2 & C_{44}+\sigma_3 & C_{24}+\sigma_4 & C_{46}+\sigma_5 & C_{26}+\sigma_6 \\ C_{55}+\sigma_1 & C_{44}+\sigma_2 & C_{33}+\sigma_3 & C_{34}+\sigma_4 & C_{35}+\sigma_5 & C_{45}+\sigma_6 \\ C_{56} & C_{24} & C_{34} & (C_{23}+C_{44})/2 & (C_{45}+C_{36})/2 & (C_{46}+C_{25})/2 \\ C_{15} & C_{46} & C_{35} & (C_{45}+C_{36})/2 & (C_{13}+C_{55})/2 & (C_{14}+C_{56})/2 \\ C_{16} & C_{26} & C_{45} & (C_{46}+C_{25})/2 & (C_{14}+C_{56})/2 & (C_{12}+C_{66})/2 \end{bmatrix} \tag{19.36}$$

where all $[\tilde{C}_{\alpha\beta}]$ elements are evaluated in the initial state **X**. Comparison of Eq. 19.36 with $[K_{\alpha\beta}]$ in Eq. 19.21 indicates that many elements of $[K_{\alpha\beta}]$ are respectively equal to an individual element of $[\tilde{C}_{\alpha\beta}]$ and the rest of the $[K_{\alpha\beta}]$ elements can be simply expressed as a linear combination of two elements of $[\tilde{C}_{\alpha\beta}]$. Thus, if one obtains $[\tilde{C}_{\alpha\beta}]$ from the phase velocity measurements via Eqs. 19.34 and 19.35, all the elements of $[K_{\alpha\beta}]$ can also be determined from the $[\tilde{C}_{\alpha\beta}]$ coefficients.

19.4.2. Formulas for a Stressed Orthotropic Medium

An isotropic material in the stress-free natural state behaves under unequal biaxial or triaxial stresses as if it possessed orthorhombic symmetry, which is characterized as satisfying the zero Huang's condition. A material of cubic, tetragonal, or orthorhombic symmetry in the natural state behaves under unequal biaxial or triaxial stresses also like one of orthorhombic symmetry but not exactly, when the principal stress or strain directions coincide with those of the material symmetry in the natural state. However, these materials under biaxial or triaxial stresses satisfy the nonzero Huang's conditions (Eq. 19.33). Such materials, which obey the nonzero Huang's conditions, are said to possess orthotropic symmetry. We choose the principal stress directions in an orthotropic material as the coordinate system. Then $\sigma_{ij} = \sigma_i \delta_{ij}$ (i not summed; $i = 1, 2, 3$) and $\zeta_{ij}(\mathbf{X}; \mathbf{a}) = \zeta_i(\mathbf{X}; \mathbf{a})\delta_{ij}$ (i not summed), where σ_i and $\zeta_i(\mathbf{X}; \mathbf{a})$ denote a principal stress and a principal strain, respectively. For an orthotropic medium, there are a total of 9 nonzero independent $[C_{\alpha\beta}]$ elements: C_{11}, C_{12}, C_{13}, C_{22} C_{23}, C_{33}, C_{44}, C_{55}, C_{66}, and there are a total of 12 nonzero $[K_{\alpha\beta}]$ elements: K_{11}, K_{12}, K_{13}, K_{21}, K_{22}, K_{23}, K_{31}, K_{32}, K_{33}, K_{44}, K_{55}, and K_{66}, among which 11 are independent, because the Huang's condition $K_{12} - K_{21} + K_{23} - K_{32} + K_{31} - K_{13} = 0$, as can be seen in Eq. 19.20, holds. An isotropic material in the natural state behaves under two equal ($\sigma_1 = \sigma_2$, which may be zero) principal stresses and one unequal nonzero principal stress σ_3 as a transversely isotropic material with nonzero Huang's conditions. The transversely isotropic material in this case has five $[C_{\alpha\beta}]$ elements: $C_{11} = C_{22}$,

C_{12}, $C_{13} = C_{23}$, C_{33}, $C_{44} = C_{55}$, $C_{66} = (C_{11} - C_{12})/2$. It is considered a special case of orthotropic symmetry.

Explicit analytic expressions for $[K_{\alpha\beta}]$ elements in terms of phase velocity can be easily derived for stressed media with orthotropic or higher symmetry, where the principal stress directions coincide with those of material symmetry and are chosen as the coordinate system. Eqs. 19.35 and 19.36 indicate that for a plane wave propagating in the direction of the principal axes of orthotropic symmetry, the wave motion is either pure longitudinal or pure transverse. Nine wave speeds V_{ij} propagating along the X_j direction with polarization in the X_i direction are conveniently placed as the ij elements in matrix form as

$$[\rho_X V_{ij}^2] = \begin{bmatrix} \tilde{C}_{11} & \tilde{C}_{12} & \tilde{C}_{13} \\ \tilde{C}_{21} & \tilde{C}_{22} & \tilde{C}_{23} \\ \tilde{C}_{31} & \tilde{C}_{32} & \tilde{C}_{33} \end{bmatrix} \tag{19.37}$$

$$\frac{1}{2}\rho_X[(V_{ij}^2 + V_{ji}^2)] = \begin{bmatrix} K_{11}^S & K_{66}^S & K_{55}^S \\ K_{66}^S & K_{22}^S & K_{44}^S \\ K_{55}^S & K_{44}^S & K_{33}^S \end{bmatrix} \tag{19.38}$$

Once the diagonal elements of $[K_{\alpha\beta}]$ are determined via Eq. 19.38 from the measurements of phase velocities propagating along the symmetry directions, the off-diagonal elements of $[K_{\alpha\beta}]$ can be obtained from the phase velocity measurements of quasi-longitudinal (QL) and quasi-transverse (QT) modes traveling in an oblique direction on the symmetry plane of an orthotropic medium. For example, both K_{13}^S and K_{31}^S can be calculated from the phase velocities of the QL and QT waves propagating at an angle θ to the X_3 axis in the X_1X_3 plane. In this case the solution of Eq. 19.35 yields

$$\begin{aligned} 2V_{QL/QT}^2 = {} & (V_{11}^2 + V_{31}^2)\sin^2\theta + (V_{33}^2 + V_{13}^2)\cos^2\theta \\ & \pm \{[(V_{11}^2 - V_{31}^2)\sin^2\theta - (V_{33}^2 - V_{13}^2)\cos^2\theta]^2 \\ & + 4[(K_{13}^S/\rho_X) + V_{31}^2]^2 \sin^2\theta\cos^2\theta\}^{1/2} \end{aligned} \tag{19.39}$$

$$\begin{aligned} 2V_{QL/QT}^2 = {} & (V_{11}^2 + V_{31}^2)\sin^2\theta + (V_{33}^2 + V_{13}^2)\cos^2\theta \\ & \pm \{[(V_{11}^2 - V_{31}^2)\sin^2\theta - (V_{33}^2 - V_{13}^2)\cos^2\theta]^2 \\ & + 4[(K_{31}^S/\rho_X) + V_{13}^2]^2 \sin^2\theta\cos^2\theta\}^{1/2} \end{aligned} \tag{19.40}$$

where $\pm$ signs in front of the curly bracket correspond to the QL and QT modes, respectively. Expressions involving K_{12}^S, K_{21}^S and K_{23}^S, K_{32}^S are obtained by the proper rotation of indices in Eqs. 19.39 and 19.40.

Effective shear moduli $K_{\alpha\alpha}^S$ (α not summed; $\alpha = 4, 5, 6$) can also be determined from shear-horizontally (SH) polarized, pure transverse (PT) modes propagating in an oblique direction on the symmetry plane of an orthotropic medium. For a PT wave propagating at an angle θ to the X_3 axis in the X_1X_3 plane with SH polarization in the X_2 direction, the PT phase velocity V_{25} is given by

$$\rho_X V_{25}^2(\theta) = \tilde{C}_{21}\sin^2\theta + \tilde{C}_{23}\cos^2\theta \tag{19.41}$$

Similarly, the phase velocity of a PT mode propagating at an angle θ to the X_3 axis in the X_2X_3 plane with SH polarization in the X_1 direction is expressed as

$$\rho_X V_{14}^2(\theta) = \tilde{C}_{12}\sin^2\theta + \tilde{C}_{13}\cos^2\theta \tag{19.42}$$

In Eqs. 19.41 and 19.42, the first subscripts 2 and 1 of V denote the X_2 and X_1 polarization directions, respectively, and the second subscripts 5 and 4 of V represent the

X_1X_3 and X_2X_3 planes, respectively. Addition and subtraction of these two equations yield

$$\rho_X[V_{14}^2(\theta) + V_{25}^2(\theta)] = 2K_{66}^S \sin^2\theta + [\rho_X(V_{13}^2 + V_{23}^2)]\cos^2\theta \tag{19.43}$$

$$\rho_X[V_{14}^2(\theta) - V_{25}^2(\theta)] = [\rho_X(V_{12}^2 - V_{21}^2)](1 + \sin^2\theta)/2 + (K_{55}^S - K_{44}^S)\cos^2\theta \tag{19.44}$$

By measuring the phase velocities of SH polarized PT modes along at least two different directions in the X_1X_3 and X_2X_3 planes, both K_{66}^S and $K_{55}^S - K_{44}^S$ can be determined via Eqs. 19.43 and 19.44, respectively. K_{44}^S and K_{55}^S can both be obtained similarly by measuring the SH polarized PT phase velocities V_{36} in the X_1X_2 plane.

Some of Huang's conditions are known as the birefringence formulas in acoustoelasticity, which are written as

$$\begin{aligned} \tilde{C}_{12} - \tilde{C}_{21} &= K_{12} - K_{21} = \sigma_2 - \sigma_1 \\ \tilde{C}_{23} - \tilde{C}_{32} &= K_{23} - K_{32} = \sigma_3 - \sigma_2 \\ \tilde{C}_{13} - \tilde{C}_{31} &= K_{13} - K_{31} = \sigma_3 - \sigma_1 \end{aligned} \tag{19.45}$$

It follows from Eqs. 19.36 and 19.37 that in the cases of PT waves propagating in the principal stress directions of orthotropic media mentioned previously, Eq. 19.45 becomes

$$\begin{aligned} &\text{(a)} \quad \sigma_2 - \sigma_1 = \rho_X(V_{12}^2 - V_{21}^2) \quad \text{(b)} \quad \sigma_3 - \sigma_2 = \rho_X(V_{23}^2 - V_{32}^2) \\ &\text{(c)} \quad \sigma_3 - \sigma_1 = \rho_X(V_{13}^2 - V_{31}^2) \end{aligned} \tag{19.46}$$

More details and additional considerations on birefringence of stressed media are provided by Tokuoka and Iwashimizu [19], Tokuoka and Saito [20], and Iwashimizu and Kubomura [21]. Some useful acoustoelastic formulas for the case of a plate subjected to biaxial plane stresses are found in the article by King and Fortunko [22].

For the homogeneously stressed orthotropic specimen previously considered, in which the principal stress or strain directions coincide with those of orthotropic symmetry, it is convenient to introduce principal stretches λ_i defined as

$$\lambda_i \delta_{ij} = \partial X_i / \partial a_j \ (i \text{ not summed}) \tag{19.47}$$

Principal strain and volume V (or density ρ) change are expressed in terms of λ_i as

$$\zeta_i(\mathbf{X}; \mathbf{a}) = (\lambda_i^2 - 1)/2 \tag{19.48}$$

$$J = \left\| \frac{\partial(X_1, X_2, X_3)}{\partial(a_1, a_2, a_3)} \right\| = \frac{V_X}{V_a} = \frac{\rho_a}{\rho_X} = \lambda_1\lambda_2\lambda_3 \tag{19.49}$$

where J is the Jacobian determinant. Then the effective elastic stiffness coefficients $K_{ijkl}(\mathbf{X})$ are completely determined from measurements of the phase velocities and principal stretches λ_i. Both $C_{ijkl}(\mathbf{X})$ and $\sigma_{ij}(\mathbf{X})$, appearing, respectively, in Eq. 19.14 and Eq. 19.17, are simplified to

$$\begin{aligned} C_{ijkl}(\mathbf{X}) &= J^{-1}\lambda_i\lambda_j\lambda_k\lambda_l C_{ijkl}(\mathbf{X}; \mathbf{a}) \\ &= J^{-1}\lambda_i\lambda_j\lambda_k\lambda_l \left[C_{ijkl}(\mathbf{a}) + (1/2)C_{ijklrr}(\mathbf{a})(\lambda_r^2 - 1) + \ldots\right] \\ &\quad (i, j, k, l \text{ fixed}) \end{aligned} \tag{19.50}$$

$$\begin{aligned} \sigma_i(\mathbf{X}) &= (1/2)J^{-1}\lambda_i^2 \left[C_{ij}(\mathbf{a})(\lambda_j^2 - 1) + (1/4)C_{ijk}(\mathbf{a})(\lambda_j^2 - 1)(\lambda_k^2 - 1) + \ldots\right] \\ &\quad (i \text{ fixed}) \end{aligned} \tag{19.51}$$

$$\zeta_i(\mathbf{X};\mathbf{a}) = (\lambda_i^2 - 1)/2 = S_{ij}(\mathbf{a})\tau_j(\mathbf{X};\mathbf{a}) + (1/2)S_{ijk}(\mathbf{a})\tau_j(\mathbf{X};\mathbf{a})\tau_k(\mathbf{X};\mathbf{a}) + \ldots$$
$$= J\left[S_{ij}(\mathbf{a})\sigma_j(\mathbf{X})\lambda_j^{-2} + (1/2)JS_{ijk}(\mathbf{a})\sigma_j(\mathbf{X})\sigma_k(\mathbf{X})\lambda_j^{-2}\lambda_k^{-2} + \ldots\right]$$
(i fixed) (19.52)

The measured $K_{ijkl}(\mathbf{X})$ are related to the SOEC, TOEC, and λ_i via Eqs. 19.21, 19.50, and 19.51. If one is able to invert Eqs. 19.51 and 19.52 to express λ_i in terms of the SOEC, TOEC, and the principal Cauchy stresses σ_m ($m = 1, 2, 3$), both $C_{ijkl}(\mathbf{X})$ and $K_{ijkl}(\mathbf{X})$ can be expressed in terms of the SOEC, TOEC, and the principal Cauchy stresses. The analytical inversion is generally difficult to carry out. Rather, one may choose to expand $\zeta_i(\mathbf{X};\mathbf{a})$ or $(\lambda_i^2 - 1)$ in a Taylor series of $\sigma_j(\mathbf{X})/E_j(\mathbf{a})(j = 1, 2, 3)$, where $E_j(\mathbf{a})$ is the Young's modulus of the material in the X_j direction in the natural state, and then one tries to find the coefficients of the leading terms in terms of the SOEC and TOEC.

Once all the elements of $[K^S_{\alpha\beta}]$ are determined from the phase velocity measurements, the elastic compliance $[Q^S_{\alpha\beta}]$ is obtained as its inverse matrix. Then use is made by Kim *et al.* [2, 23] of the expressions for the Young's modulus and Poisson's ratio for orthotropic media in terms of $[K_{\alpha\beta}]$ elements. To find the Young's modulus E_3 and the Poisson's ratios ν_{13} and ν_{23} in the initial state, a small additional homogeneous loading, which is described by $\delta\sigma_{ij} = \delta\sigma_3(\mathbf{x})$ and $u_{ij} = \varepsilon_i(\mathbf{x};\mathbf{a})\delta_{ij}$ (i not summed), is superposed on the initial state along the principal X_3 direction. The terms ν_{13}, ν_{23}, and E_3 can then be written as

$$\nu_{13} \equiv -\left(\frac{\varepsilon_1}{\varepsilon_3}\right)_{\mathbf{X}} = -\left[\frac{d\lambda_1/\lambda_1}{d\lambda_3/\lambda_3}\right]_{\mathbf{X}} = -\frac{Q_{13}}{Q_{33}}$$
$$= -\frac{(\mathbf{K}^{-1})_{13}}{(\mathbf{K}^{-1})_{33}} = \frac{K_{13}K_{22} - K_{12}K_{23}}{K_{11}K_{22} - K_{12}K_{21}} \tag{19.53}$$

$$\nu_{23} \equiv -\left[\frac{\varepsilon_2}{\varepsilon_3}\right]_{\mathbf{X}} = -\left[\frac{d\lambda_2/\lambda_2}{d\lambda_3/\lambda_3}\right]_{\mathbf{X}} = -\frac{Q_{23}}{Q_{33}}$$
$$= -\frac{(\mathbf{K}^{-1})_{23}}{(\mathbf{K}^{-1})_{33}} = \frac{K_{23}K_{11} - K_{21}K_{13}}{K_{11}K_{22} - K_{12}K_{21}} \tag{19.54}$$

$$E_3 \equiv \left(\frac{d\sigma_3}{d\varepsilon_3}\right)_{\mathbf{X}} = \left[\frac{d(\delta\sigma_3)}{d\lambda_3/\lambda_3}\right]_{\mathbf{X}} = \frac{1}{Q_{33}} = \frac{1}{(\mathbf{K}^{-1})_{33}}$$
$$= K_{33} - \nu_{13}K_{31} - \nu_{23}K_{32} \tag{19.55}$$

where $K_{\alpha\beta}$ elements are given in terms of $C_{\alpha\beta}$ and σ_i in Eq. 19.21. The Young's moduli and Poisson's ratios in the X_1 and X_2 directions, E_1, E_2, ν_{21}, ν_{31}, ν_{12}, and ν_{32}, can be similarly obtained. Note that $\nu_{ij}E_j \neq \nu_{ji}E_i (i \neq j)$ in the initially stressed state, while they are equal for a medium of orthorhombic or higher symmetry in the natural state. These quantities can be also expressed in terms of the SOEC and TOEC of a material via Eqs. 19.21, 19.50, and 19.51. Numerous thermodynamic relations in a stressed state are also listed in [2], which includes the difference between the adiabatic and isothermal values of $C_{\alpha\beta}$, $K_{\alpha\beta}$, and $Q_{\alpha\beta}$, the bulk and Young's moduli, and Poisson's ratio in a stressed state. The group velocity formulas in terms of the $[K_{\alpha\beta}]$ elements for an arbitrary direction on the symmetry planes of stressed media with orthotropic or higher symmetry are given by Kim *et al.* [24]. Group velocities are usually measured by a point source–point receiver technique, described in detail in Chapter 4.

Many ultrasonic measurements of actual velocity V in lieu of the effective elastic coefficients $K_{\alpha\beta}$ in orthotropic media were made to obtain the acoustoelastic constants

necessary for estimation of the residual stresses locked in structures, in which nondestructive access to the natural configuration is very difficult to obtain. A detailed description of ultrasonic measurements of residual stresses is found in the review by Pao *et al.* [25]. Additional considerations of acoustoelastic waves in orthotropic media are described in an article by Pao and Gamer [26].

19.4.3. Effective Elastic Coefficients Under Hydrostatic Pressure

When a stressed medium is under hydrostatic pressure p, i.e., $\sigma_{ij} = -p\delta_{ij}$, the K_{ijkl} coefficients in Eq. 19.18 reduce to

$$\beta_{ijkl} = C_{ijkl} + p(\delta_{ij}\delta_{kl} - \delta_{ik}\delta_{jl} - \delta_{il}\delta_{jk}) \tag{19.56}$$

It is readily verified that the β_{ijkl} coefficients satisfy the full symmetry relations found in the SOEC $C_{ijkl}(\mathbf{a})$ defined in the stress-free natural state. The phase velocity equations corresponding to the Christoffel equation (Eq. 19.30) are obtained by replacing $C_{ijkl}(\mathbf{a})$ by β_{ijkl} in the Christoffel tensor, the wave normal $\mathbf{m}$ by $\mathbf{n}$, and the density ρ_a by ρ_X. The elements of $[\beta_{\alpha\beta}]$ are obtained by simply setting $\sigma_1 = \sigma_2 = \sigma_3 = -p$ and $\sigma_4 = \sigma_5 = \sigma_6 = 0$ in the $K_{\alpha\beta}$ elements shown in Eq. 19.21. An early ultrasonic measurement of the $[\beta_{\alpha\beta}]$ of some cubic crystals under hydrostatic pressures was achieved by Lazarus [27]. The elastic coefficients and their pressure derivatives ordinarily quoted in the literature, e.g., [16,28], are neither the thermodynamic coefficients nor their pressure derivatives, but are $[\beta_{\alpha\beta}(\mathbf{X})]$ and $\partial\beta_{\alpha\beta}/\partial p$, respectively. $[\beta_{\alpha\beta}(\mathbf{X})]$ are commonly denoted by using upper- or lower-case "cee" in the literature.

The compressibility χ in the initial state, which is the reciprocal of the bulk modulus $B(\mathbf{X})$, is expressed as

$$\chi = \frac{1}{B} = \frac{1}{\rho}\left(\frac{\partial\rho}{\partial p}\right)_{\mathbf{x}} = Q_{iikk} = Q_{11} + Q_{22} + Q_{33} + 2(Q_{12} + Q_{23} + Q_{13}) \tag{19.57}$$

where the effective compliance $Q_{\alpha\beta}$ elements are now obtained as the elements of the inverse matrix $[\beta_{\alpha\beta}(\mathbf{X})]^{-1}$ and the symmetry property $Q_{\alpha\beta} = Q_{\beta\alpha}$ under hydrostatic pressure is utilized. Under hydrostatic pressure, the symmetry of a material and its crystal structure are preserved. For all crystal classes except monoclinic and triclinic systems, one finds

$$(d\lambda_i/dp)_{p=0} = (d\zeta_i/dp)_{p=0} = -[Q_{i1}(\mathbf{a}) + Q_{i2}(\mathbf{a}) + Q_{i3}(\mathbf{a})] \tag{19.58}$$

where $Q_{ij}(\mathbf{a}) = Q_{ij}(\mathbf{a};\mathbf{a})(i, j = 1, 2, 3)$ are the zero pressure effective compliance coefficients. Note that in the natural state, $Q_{\alpha\beta}(\mathbf{a}) = S_{\alpha\beta}(\mathbf{a})$, where $S_{\alpha\beta}(\mathbf{a})$ are the thermodynamic elastic compliance coefficients at zero pressure. Applying Eqs. 19.21 and 19.50 to the case of hydrostatic pressure, the difference between the pressure derivatives of the effective and thermodynamic elastic coefficients $(d/dp)[\beta_{\alpha\beta}(\mathbf{X}) - C_{\alpha\beta}(\mathbf{X};\mathbf{a})]_{p=0}$ can be evaluated in terms of the $S_{ij}(\mathbf{a}) = S_{ij}(\mathbf{a};\mathbf{a})$ and the SOEC $C^T_{\alpha\beta}(\mathbf{a}) = C^T_{\alpha\beta}(\mathbf{a};\mathbf{a})$. The difference is given in Table II of [8]. For materials of both isotropic and cubic symmetry, the linear compressibility under hydrostatic pressure is the same in every direction. Therefore, it follows that $\lambda = \lambda_1 = \lambda_2 = \lambda_3$ and $\zeta(\mathbf{X};\mathbf{a}) = \zeta_1(\mathbf{X};\mathbf{a}) = \zeta_2(\mathbf{X};\mathbf{a}) = \zeta_3(\mathbf{X};\mathbf{a})$. The bulk modulus of a cubic material in the initial state then simplifies to

$$B = [3(Q_{11} + 2Q_{12})]^{-1} = (1/3)(\beta_{11} + 2\beta_{12}) = \beta_{11} - 4\beta'/3 = (1/3)(C_{11} + 2C_{12} + p) \tag{19.59}$$

where the adiabatic shear modulus

$$\beta'^S = (\beta^S_{11} - \beta^S_{12})/2 = \rho_X V_T^2 \tag{19.60}$$

can be determined from the phase velocity V_T of a pure transverse wave traveling along the $< 110 >$ direction and polarized in the $< 1\bar{1}0 >$ direction of a cubic crystal. Detailed ultrasonic measurements under high pressure are provided in Chapter 20 by Bassett.

19.4.4. Experimental Methods for Measuring Effective Elastic Coefficients

It is noted that determination of $K_{ijkl}(\mathbf{X})$ coefficients from phase velocity measurements also requires knowledge of the actual acoustic path length L_X and the density ρ_X in the stressed initial state, since only transit times τ of sound waves are usually measured in ultrasonic experiments. Because the initial state is static, both L_X and ρ_X are usually determined by static measurements of the principal stretches λ_i or the dimensional change of a specimen. The static measurement techniques for dimensional change lie outside the scope of this chapter. Under hydrostatic pressures, the relations for density or volume change versus pressure are known as the equations of state of solids, among which are the well-known Murnaghan's first- and second-order equations [29] and Birch's equation of state [9,30]. Cook [31] devised a clever procedure for calculating the dimensional change λ_i in cubic, hexagonal, and transversely isotropic materials at any pressure from the measured ultrasonic transit time data versus pressure and the knowledge of dimensions and the density in the reference state. Thurston [32] calculated changes in lattice parameter or λ_i with hydrostatic pressure from the SOEC and TOEC data of materials having various crystal symmetries. Analogous nonlinear equations of state under uniaxial homogeneous loading for cubic and isotropic materials, say, in the X_3 direction, have recently been provided by Kim and Sachse [33], who expressed $\sigma_{33}(\mathbf{X})$, Poisson's ratio, Young's modulus, and ρ_X/ρ_a in terms of the strain $\varepsilon_{33}(\mathbf{X};\mathbf{a})$ or λ_3, the SOEC, and the TOEC.

Below the elastic limit of ordinary materials, such as strong metals, ceramics, and covalent materials, a fractional change in transit time τ is quite small and is typically an order of a few percent. However, this is not the case under high hydrostatic pressures, which suppress plastic deformation and can thus be applied well over 400 GPa [34], under which the elastic constants may well change by many times their atmospheric values. Even under hydrostatic pressures under 1 GPa, a fractional change in transit time is substantial for soft materials such as alkali metals and some alkali halides. For the universal detection of a small change in transit time under a general stress, it is essential to use ultrasonic instrumentation that provides high accuracy in transit time measurement.

A variety of ultrasonic techniques capable of accurately measuring transit times have been developed over the last half-century. Details of some of these methods are provided in Chapter 2 by Papadakis. Most of the accurate measurement techniques are based either on resonance or on interference of ultrasonic beams that reverberate inside two parallel opposite faces of a specimen. Here we briefly mention five different techniques that provide an accuracy in τ measurement better than one part in 10^4 in their refined forms and that can be easily adapted for transit time measurements under a general stress. The Brillouin scattering technique, which lacks accuracy in sound speed measurement, is also mentioned because it may be the only possible technique for measuring the elastic constants of a tiny sample of size less than 0.1 mm^3 under very high pressure inside a diamond anvil cell, where electrical feed-through and attaching acoustic transducers are difficult to realize. Very large changes in elastic constants that may be many times those at atmospheric pressure override the lack of accuracy in sound speed measurements in the Brillouin technique.

19.4.4.1. Phase Comparison Method

The phase comparison method developed by Williams and Lamb [35] uses the double pulses generated by double gates. The double pulses with the same rf carrier frequency

with a much lower pulse repetition rate are applied to a transducer that is directly bonded to a specimen. A gate 1 is first opened and an rf burst signal is applied to the transducer, which results in the echo trains. The time at which gate 2 opens is delayed by nearly one round-trip interval, so that echoes are aligned and are superposed to interfere with each other. The carrier rf frequency is varied until phase cancellation occurs, and a sequence of nulls is produced by destructive interference by adjusting a carrier frequency. From the sequence of the carrier null frequencies the phase velocity of a specimen is calculated following the analysis by Williams and Lamb. An advantage with this method is that it can take care of the phase shift due to the bond of the transducer on the specimen, and the null frequency of the rf (about 10 MHz) carrier can be determined with high precision.

19.4.4.2. Pulse Superposition Method

The pulse superposition method developed by McSkimin [36, 37] differs from the phase comparison method in that the pulse repetition frequency (PRF) of the pulse oscillator is crucial to the constructive interference among the successive echoes and the measurement of transit time τ, rather than the frequency of carrier. The cw oscillator of carrier frequency is pulsed by the pulse repetition oscillator at a PRF of 1 MHz or less and drives the transducer. In principle, the period of the PRF is adjusted to be equal to some integral number of round trips in a specimen. When this condition is achieved, the applied pulses are superposed on the specimen echoes. In practice, it is preferable to operate with this integer equal to unity, for then the greatest amount of energy is impressed upon the specimen. To observe the echoes on an oscilloscope, a window is placed in the sequence of applied pulses by applying a gating voltage derived from the oscilloscope to the pulsed oscillator. Then one adjusts the PRF to maximize the amplitude of the observed echoes. The measured period of the PRF, equal to the reciprocal of the PRF, is related to the transit time τ by the formula described by McSkimin, who provided correction for the phase shift due to the bond of the transducer to the specimen.

19.4.4.3. Pulse-Echo-Overlap Method

This method is described in detail in the article written by Papadakis [38]. Two echo signals of interest are made to overlap in the oscilloscope by driving the x axis with a cw oscillator signal having a period equal to the travel time between the echoes. One signal appears on one sweep of the oscilloscope, and the other signal appears on the next sweep. The sync input of the oscilloscope is connected to the pulser triggered by a frequency divider that divides the cw frequency by a large integer, e.g., 1000. The pulser also drives the transducer attached to the sample. The echoes are amplified, fed into the y axis of the scope, and displayed on the screen. Then the cw frequency is adjusted such that the observed echoes are precisely overlapped. The round-trip travel time of the echoes is a reciprocal of the cw frequency.

19.4.4.4. Sing-Around Method

In this system, two ultrasonic transducers, one acting as a transmitter and the other as a receiver, are directly bonded to the opposite faces of a specimen. The essential idea is to employ a signal from the receiving transducer in a feedback loop that triggers the pulse generator so as to establish a pulse repetition frequency (PRF) at which a pulsed signal is sent to a transmitter. When a steady-state condition is established, the PRF is nearly $1/\tau$. A greatly improved version was developed by Forgacs [39], who introduced a second gate that selected one of the multiply reflected pulse echoes. When

the n'th echo is selected, it has traveled a specimen $(2n-1)$ times, resulting both in an increase of the effective length of the specimen and in attenuation of the signal that triggers the next pulse.

19.4.4.5. Continuous Wave (CW) Resonance Method

In the basic CW technique developed by Bolef and Miller [40], both transmitting and receiving transducers attached on opposite sides of a specimen are continuously driven by the signals derived from a cw oscillator. Observation is begun only after a steady state has been reached. As one sweeps the frequency of the cw oscillator, the frequency spectrum of the received signal amplitude exhibits sharp peaks at frequencies corresponding to the mechanical resonances that occur at integral multiples of half-wavelengths of ultrasound. Actually, the specimen, transmitter, and receiver constitute a composite oscillator. The problem of the electromagnetic crosstalk between the transmitter and receiver has been eliminated in a sampled CW technique [41], which gates a cw oscillator sufficiently long enough to establish a steady-state condition in the specimen. Then the transmitter is gated off and the receiver is gated on to observe a decay response of the transient signal on a sampling oscilloscope. A frequency spectrum that displays sharp mechanical resonances is obtained as the transmitter frequency is swept over the region of interest. Petersen *et al.* [42] improved the sampled CW technique of Bolef and Miller by adopting up-to-date instrumentation with the superheterodyne phase-sensitive *detector* and gated integrator, which process a decaying signal to provide the amplitude and phase of the signal after the transmitter gate is off. Their system works well with noncontact EMATs (electromagnetic acoustic transducers), which require no coupling correction for an absolute τ measurement. The principles of the EMAT system are described by Dobbs [43], and the acoustoelastic measurements using EMATs are given in detail in Chapter 11 by Alers and Ogi. The EMAT system requires an electrically conducting surface of a specimen.

19.4.4.6. Brillouin Scattering Method

In this method [44], incident beams generated from a laser source pass through a sample. The Brillouin frequency shift due to light scattering by thermal phonons of the specimen is measured by employing some type of spectrometer or multipass Fabry-Perot type of interferometer. The sound speed is calculated from the Brillouin frequency shift data. The density of a specimen under high pressure is usually separately measured by adopting an x-ray diffraction technique. The effective elastic constants are calculated from the density, and sound velocity data thus obtained. This method is explained in detail in Chapter 14 by Grimsditch.

19.4.5. Illustrations of Acoustoelastic Behavior

There have been numerous measurements of acoustoelasticity using one of the measurement techniques described in the previous section. Since the early 1970s many authors have performed measurements under uniaxial or biaxial stresses in an attempt to determine residual stresses [25]. Numerous measurements using either hydrostatic pressure or both hydrostatic and uniaxial stresses were carried out after the Second World War to study the properties of matter under high compressive stress [16]. Here we mention a few examples that exhibit distinctly acoustoelastic phenomena.

Figure 19.1 shows the measurements of Egle and Bray [45], which display the changes in the sound speed of five different modes in a specimen of railroad steel under uniaxial loading in the axial direction X_1. The steel was isotropic in the stress-free natural state and behaves as a transversely isotropic material under the uniaxial stress

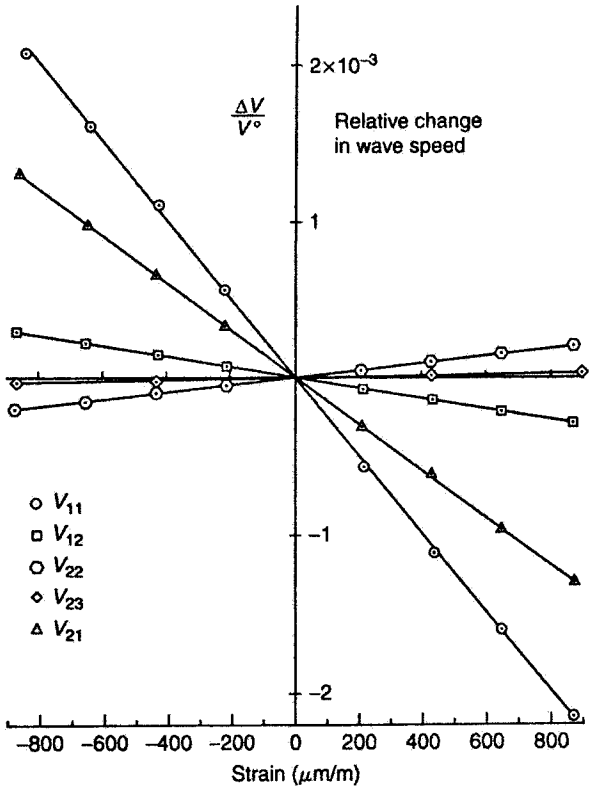

Fig. 19.1. Relative change in wave speed as a function of strain in a railroad steel specimen loaded along the X_1 direction. The first and second subscript indices in V denote propagation and polarization directions, respectively, and these notations are opposite to those used in the text (from Egle and Bray [45]).

($\sigma_1 \neq 0$, $\sigma_2 = \sigma_3 = 0$). The Young's modulus E_0 and the Poisson's ratio ν_0 of the steel in the natural state are respectively, 207 GPa and 0.296. In Figure 19.1, the first and second subscripts in V_{ij} $(i, j = 1, 2,$ or 3) indicate the directions of propagation and the polarization of sound waves, respectively. As one might expect from Eqs. 19.36, 19.37, 19.38, 19.50, and 19.51, in a small stress range below the elastic limit of a steel, the changes in sound velocities are small and linear with respect to strain or stress. Each line in Figure 19.1 can be fit into the formulas developed by Hughes and Kelly [13] to determine the TOEC of the railroad steel. It follows from the birefringence formulas, Eqs. 19.45 and 19.46, that when the changes in V_{12} and V_{21} are small, the difference in them can be approximated by

$$(\delta V_{12} - \delta V_{21})/V_S^0 = (V_{12} - V_{21})/V_S^0 \cong A(\sigma_1 - \sigma_2) = A\sigma_1 \cong A\varepsilon_1(\mathbf{X}; \mathbf{a})/E_0 \quad (19.61)$$

where A is called the acoustoelastic constant, which can be expressed in terms of the SOEC and TOEC [13,25], and V_S^0 is the shear wave speed in the stress-free state. In Figure 19.1 the acoustoelastic constant A of the railroad steel is found to be $0.0064(\text{GPa})^{-1}$.

Hsu [46] generated two-dimensional inhomogeneous stress fields in two aluminum disks by compressing diametrically along the uniaxial direction X_1. The differences between biaxial principal stresses, $\sigma_1 - \sigma_2$, are obtained from the measured shear wave speeds, V_{12} and V_{21}, and the acoustoelastic constant A (refer to Eq. 19.61) obtained from uniaxial homogeneous stress tests. The pulse-echo-overlap method [38] was used to measure the ultrasonic transit times. The size of the shear transducer is relatively small in comparison with the diameter of the disk. As shown in Figure 19.2, the

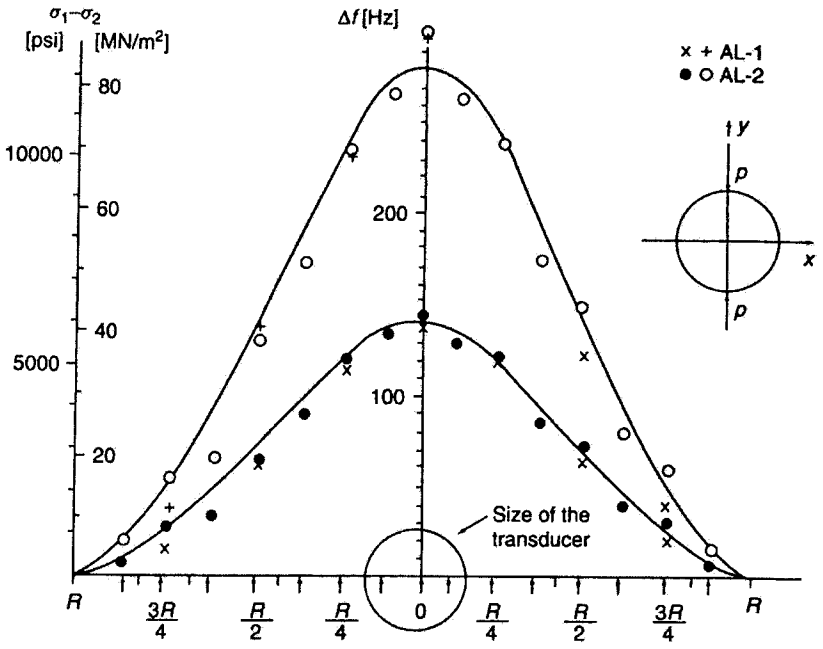

Fig. 19.2. Distribution of $(\sigma_1 - \sigma_2)$ along a horizontal diameter of two aluminum disks under vertical diametric compression. Solid lines are calculated according to linear elasticity theory. Points are measured triggering-frequency differences; arrows on the horizontal axis indicate the location of the center of the transducer during the test (from Hsu [46]).

measured differences $\sigma_1 - \sigma_2$ are generally in good agreement with the values predicted from linear elasticity theory. Okada [47] carried out an acoustoelastic determination of stress in slightly orthotropic materials using orthotropic acoustoelastic relations and the equations of equilibrium in the initial state.

It is noted that a material, after it undergoes plastic deformation, is no longer considered to be the same material with the same structure in the context of acoustoelasticity, unless it is a perfect single crystal free of any defects and impurities prior to plastic deformation. Plastic deformation, alters the microstructure of a material such as, defects, voids, dislocations, distribution of precipitated particles, grain size and orientation, texture, etc. Therefore, a plastically deformed material should in principle be considered a new material in the sense that it is characterized by a new set of the SOEC and HOEC, even though its overall chemical composition remains the same before and after plastic deformation. In general, the TOEC and HOEC are much more sensitive to a change in microstructure than the SOEC. One expects that the acoustoelastic constants after plastic deformation also change and may be quite sensitive to a change in the microstructure of a material. Acoustoplasticity lies outside the scope of this chapter. Readers interested in this area are referred to [25, 48–50].

What prevents one from applying very high, distinctly nonhydrostatic stresses to a material is the yielding of a material during plastic deformation. Hydrostatic pressure keeps plastic deformation from taking place, and thus very high pressures exceeding well over 100 GPa can be applied to a specimen inside a diamond anvil cell. It is usual for many insulators to transform into a metallic phase under high pressures. Other types of phase transformation, such as a change in crystal structure, order–disorder transition, a change in magnetic phase, transition from normal to superconducting phase and vice versa, solidification and melting, etc., can be induced by increasing or decreasing the pressures applied to a specimen.

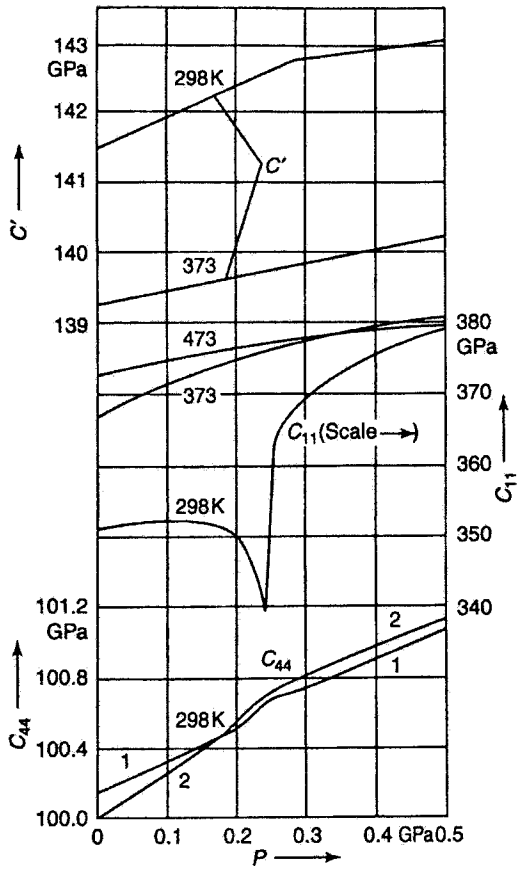

Fig. 19.3. The effective elastic coefficients $C_{\alpha\beta}$ and $C' = (C_{11} - C_{12})/2$ of BCC chromium versus pressure $p \cdot p_N$(Néel pressure) = 0.24 GPa at $T = 298\,^{\circ}$K. The numbers on the bottom curves are: 1 with propagation along [001] and polarization along [100]; 2 with propagation along [110] and polarization along [001] (from Katahara *et al.* [51]).

When a material undergoes a phase transition under compressive stresses, some of the effective elastic coefficients may exhibit an anomalous behavior, such as mode softening around the phase transition and a sharp discontinuity in the first pressure derivative at the transition pressure. Figure 19.3 shows the results of Katahara *et al.* [51], which indicate an anomalous behavior of C_{11} and the discontinuity in the first pressure derivatives of C_{44} and $C' = (C_{11} - C_{12})/2$ of BCC chromium as the pressure increases across the Néel transition pressure $p_N = 0.24$ GPa at room temperature (25 °C). The elastic constants are measured by using McSkimin's pulse superposition method [36]. BCC Cr transforms from antiferromagnetic phase at atmospheric pressure into paramagnetic phase above the Néel transition pressure. The cee's in the figure are actually effective elastic coefficients $K_{\alpha\beta}$ or $\beta_{\alpha\beta}$. A behavior similar to that displayed in $C_{11}(p)$ of Cr about p_N is found in some $C_{\alpha\beta}(T)$ of many materials that undergo phase transformation as the temperature T changes. Some alkali halides (e.g., potassium and rubidium halides) undergo Martensitic phase transformation from the NaCl structure into a CsCl structure as the pressure exceeds a phase transition pressure at room temperature. In these binary compounds the effective elastic shear coefficient β_{44} in the NaCl phase becomes anomalously softer with increasing pressure ($\partial\beta_{44}/\partial p < 0$) [16].

Figure 19.4 shows drastic changes in the three effective elastic coefficients of cubic solid krypton (Kr). The effective elastic coefficients as a function of pressure inside a diamond anvil cell were obtained by Polian *et al.* [52] using Brillouin scattering. The

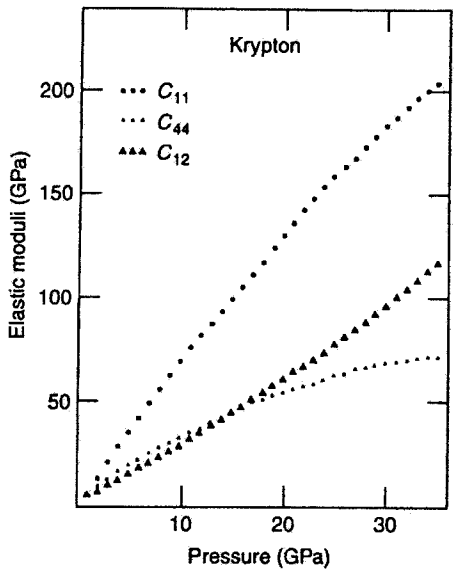

Fig. 19.4. The effective elastic coefficients (GPa) of krypton as a function of pressure (from Polian *et al.* [52]).

Brillouin frequency shift is measured by using a five-pass Fabry-Perot interferometer, and the density change or the equation of state of Kr is obtained from energy-dispersive synchrotron x-ray diffraction data. A small nonlinearity apparent in the behavior of effective elastic constants versus pressure indicates that fourth-order elastic constants should be accounted for in an acoustoelastic behavior of Kr. Above 30 GPa, C_{11} (or β_{11}) is seen to change more than 20 times over its lowest pressure values.

19.5. ABSOLUTE ACOUSTOELASTIC STRESS GAUGE

With advances both in metrology of dimensional changes λ_i and in accurate measurements of ultrasonic transit times τ, it is possible to accurately determine the absolute stress or the absolute force acting on a specimen from the first principle of definition without relying on calibration by dead weight or other means. An absolute change in dimensions is usually measured using a laser interferometer, the stabilized wavelength of which is precisely known. The ultrasonic transit times are usually obtained from measurements of resonance frequencies that are precisely calibrated either with respect to those of quartz or against the atomic clock.

In the case of hydrostatic pressure p applied on isotropic or cubic materials, p is expressed as

$$p(\mathbf{X}) = 3\int_1^{\lambda(\mathbf{X})} \frac{B^T d\lambda}{\lambda} = 3\int_1^{\lambda(\mathbf{X})} \frac{B^S d\lambda}{(1+\Delta_p)\lambda} \tag{19.62}$$

where the bulk modulus B is given in Eq. 19.59 and $\Delta_p = \beta^2 B^S T/(\rho C_p)$ is a small correction factor between the adiabatic and isothermal bulk moduli. Here β and C_p denote the bulk thermal expansion coefficient and specific heat at constant pressure, respectively. The adiabatic bulk modulus B^S is obtained as a function of λ from measurements of relevant phase velocities and dimensional change λ via Eq. 19.59. Then the absolute pressure p is calculated from Eq. 19.62. Ruoff *et al.* [53] constructed an absolute pressure based on Eq. 19.62 using a cubic silicon crystal as a specimen. It is considered one of the most accurate absolute pressure gauges.

In the case of an orthotropic specimen that is uniaxially stressed, say, in the X_3 direction, as conventionally found in a uniaxial tension and compression testing for materials characterization, the Cauchy stress $\sigma_3(\mathbf{X})$ is given via Eqs. 19.55 and 19.46c by

$$\sigma_3(\mathbf{X}) = \int_1^{\lambda_3(\mathbf{X})} \frac{E_3^T d\lambda_3}{\lambda_3} = \int_1^{\lambda_3(\mathbf{X})} \frac{E_3^S d\lambda_3}{(1+\Delta_3)\lambda_3} \tag{19.63}$$

$$\sigma_3(\mathbf{X}) = \rho_a[\lambda_1(\mathbf{X})\lambda_2(\mathbf{X})\lambda_3(\mathbf{X})]^{-1}[V_{13}^2(\mathbf{X}) - V_{31}^2(\mathbf{X})] \tag{19.64}$$

where E_3^S expressed in Eq. 19.55 can be measured as a function of λ_3 from phase velocity measurements as explained in Section 19.4.2 and Δ_3 is a small correction factor between the adiabatic and isothermal Young's moduli. The expression for Δ_3 is given in [2], and its dependence on λ_3 may be ignored. If one measures static dimensional changes including λ_3 and the relevant phase velocities of various modes accurately, $\sigma_3(\mathbf{X})$ can be obtained either from Eq. 19.63 or from Eq. 19.64. However, because of a small difference between V_{13} and V_{31} below the yield stress of a material, the accuracy in $\sigma_3(\mathbf{X})$ measurements is expected to be much higher by using Eq. 19.63 than by using Eq. 19.64. Kim and Sachse [23] developed the theory of an absolute thermodynamic–acoustoelastic stress gauge based on Eqs. 19.63 and 19.64.

Consider a biaxially stressed orthotropic medium with two nonzero principal stresses σ_1 and σ_2, ($\sigma_3 = 0$) whose directions coincide with those of material symmetry. The phase velocities of QL and QT modes propagating in an arbitrary direction on the symmetry plane, say, the X_1X_3 plane, are given by Eqs. 19.39 and 19.40, which indicate that the QL/QT phase velocities are expressed in terms of 6 parameters that include four thermodynamic elastic coefficients C_{11}, C_{33}, C_{13}, and C_{55}, the density ρ_X, and the principal stress σ_1, given that the principal directions are known. The phase velocities of QL and QT waves propagating in the biaxially stressed X_1X_2 plane, whose principal stress directions are unknown, are expressed in terms of 10 parameters that include six thermodynamic elastic coefficients C_{11}, C_{22}, C_{12}, C_{66}, C_{16}, C_{26}, the initial density ρ_X, and the stresses σ_{11}, σ_{12}, and σ_{22}. With the X_1 and X_2 directions deviating from the principal stress directions, the wave propagation in the X_1X_2 plane is characterized as having monotropic symmetry. These thermodynamic elastic coefficients, the initial density, and stresses can be obtained by a nonlinear least-squares method, using a modern high-speed computer equipped with large memory. The measured phase velocities of QL/QT waves propagating in various directions are fit to a nonlinear phase velocity equation derived from Eq. 19.27 or Eq. 19.35 to find optimal values of these multiple parameters, which minimize the sum of the square of differences between the measured and calculated phase velocities. Degtyar and Rokhlin [54] investigated the feasibility of this approach to determine the applied and residual stresses in anisotropic materials. Tempting as this approach may be, many parameters that must be determined by the nonlinear least-squares fitting and the small acoustoelastic effect of stresses on the phase velocity result in large uncertainty in some of the determined parameters, including the stresses.

19.6. ACOUSTOELASTICITY OF SURFACE ACOUSTIC WAVES

A theory of surface acoustic waves (SAWs) in a homogeneously deformed semi-infinite elastic medium was developed by Hayes and Rivlin [55], who considered also the case of Love waves in a prestressed layer over a semi-infinite medium. SAW motion is confined near the surface over a region of about one wavelength deep, and the SAW behaves as an inhomogeneous wave with its amplitude varying along the depth, as in the case of a stress-free half-space medium. The equations of motion (Eqs. 19.24 and

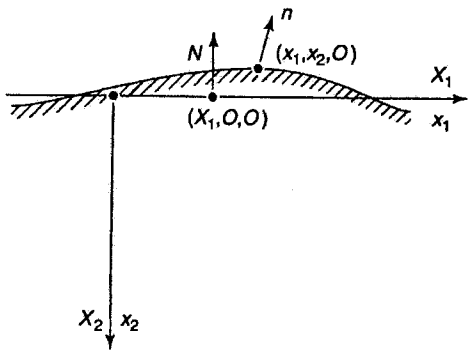

Fig. 19.5. Schematics of geometry of a surface wave over a deformed half-space.

19.32) are subjected to the constraint of a traction-free surface condition on propagation of the SAW. Let a unit outward normal to the traction-free surface be denoted by **N** in the initial state **X**. As shown in Figure 19.5, on passage of the SAW, the surface becomes slightly deformed into a traction-free wavy surface with a new unit normal **n** in the current configuration **x**. The surface boundary conditions in the initial and current configurations are stated, respectively, as $N_j\sigma_{ij}(\mathbf{X}) = 0$ and $n_j\sigma_{ij}(\mathbf{x}) = 0$, which transforms into [55, 56].

$$N_j C_{ijkl}(\mathbf{X})(\partial u_k/\partial X_l) = 0 \tag{19.65}$$

We choose the initial coordinates **X** to be aligned parallel to the directions of the three principal initial stresses σ_1, σ_2, and σ_3, and the X_2 axis to be normal to the traction-free plane surface located at $X_2 = 0$ of a semi-infinite medium occupying $X_2 \geq 0$. For an orthotropic medium as previously considered in the initial state **X**, the traction-free boundary condition Eq. 19.65 at $X_2 = 0$ can be written as

$$u_{1,2} + u_{2,1} = 0 \quad C_{1122}u_{1,1} + C_{2222}u_{2,2} = 0 \quad \text{at } X_2 = 0 \tag{19.66}$$

where $u_{i,j} = \partial u_i/\partial X_j$.

We consider a SAW propagating at phase velocity V with wave vector **k** in the X_1 direction of the orthotropic medium. In this case, wave motion of the SAW is seen to be confined in the sagittal X_1X_2 plane symmetry considerations and the SAW behaves as a Rayleigh wave (RW) mode. By seeking the solution of a form

$$u_i = f_i(X_2)\exp[ik(X_1 - Vt)] \ (i = 1, 2), \ u_3 = 0 \tag{19.67}$$

subjected to the boundary condition Eq. 19.66 for the equation of motion (Eq. 19.24 or 19.32), and discarding a degenerate case, one obtains the nontrivial solution [55].

$$\left[C^S_{22}(C^S_{11} + \sigma_1 - \rho_X V^2) - C^{S^2}_{12}\right]^2 (C^S_{66} + \sigma_1 - \rho_X V^2)$$
$$= C^S_{22}C^S_{66}(\rho_X V^2 - \sigma_1)^2(C^S_{11} + \sigma_1 - \rho_X V^2) \tag{19.68}$$

On the $X_2 = 0$ free surface, the corresponding effective elastic coefficients are $K_{11} = C_{11} + \sigma_1$, $K_{22} = C_{22}$, $K_{21} = C_{12}$, and $K_{66} = C_{66} + \sigma_1/2$, since $\sigma_2 = 0$ on the traction-free surface. It is recognized that while the explicit dependence of the RW speed on σ_1 is apparent in Eq. 19.68, the RW velocity is an implicit function of σ_3 through $C_{\alpha\beta}$, which vary with σ_1 and σ_3. The RW speed shown in Eq. 19.68 is nondispersive. In the special case of the initial state being stress-free, Eq. 19.68 becomes identical with the RW equation in an orthorhombic half-space which was derived by Stoneley [57]

and Royer and Dieulesaint [58], who considered also RW propagation along crystallographic axes of cubic, tetragonal, and transversely isotropic media and along the $< 110 >$-type directions of the former two media. The SAW propagation along the surface of stress-free anisotropic media was summarized by Farnell [59]. Note that the boundary conditions specified by Eqs. 19.65 and 19.66 for a stressed orthotropic half-space are essentially the same as those for a stress-free orthorhombic half-space if $C_{ijkl}(\mathbf{X})$ and $\mathbf{N}$ are respectively replaced by $C_{ijkl}(\mathbf{a})$ and $\mathbf{M}$, a unit outward normal to the stress-free surface. Then the Christoffel equation (Eq. 19.30) becomes equivalent to Eq. 19.27 if the eigenvalue $\rho_a V^2$ and wave normal $\mathbf{m}$ in Eq. 19.30 are respectively replaced by $\rho_X V^2 - \sigma_{jl}(\mathbf{X}) n_j n_l$ and $\mathbf{n}$. One finds that Eq. 19.68 is obtained from Stoneley's result [57] by replacing $C_{\alpha\beta}(\mathbf{a})$ and $\rho_a V^2$ by $C_{\alpha\beta}(\mathbf{X})$ and $\rho_X V^2 - \sigma_1(\mathbf{X})$, respectively.

For a small change of RW speed in a stressed medium, which is isotropic in the natural state, Hayes and Rivlin [55] assumed in Eq. 19.68 the following dependence of the RW speed V along the principal stress direction on two independent principal strains:

$$\rho_X V^2 = \rho_a V_0^2 + \alpha_1 \varepsilon_{11} + \alpha_2 \varepsilon_{22} \tag{19.69}$$

and expressed a fractional change in RW speed, $\Delta V/V_0$, as

$$\frac{\Delta V}{V_0} = \frac{V - V_0}{V_0} = \frac{\alpha_1}{2\rho_a V_0^2} \varepsilon_{11}(\mathbf{X};\mathbf{a}) + \left(\frac{\alpha_2}{2\rho_a V_0^2} - \frac{\mu}{\lambda} \right) \varepsilon_{22}(\mathbf{X};\mathbf{a}) \tag{19.70}$$

where V_0, λ, and μ are, respectively, the RW speed and the Lamé constants in the natural state $\mathbf{a}$, ε_{11} and ε_{22} are the principal nominal strains (see Eq. 19.3), and α_1 and α_2 are the constants determined from a complicated set of equations that involve the SOEC and TOEC [55].

Hayes and Rivlin's result (Eq. 19.70) was first applied to study variations of RW speed with uniaxially applied stress σ_1 in an experiment by Hirao *et al.* [60], who used the sing-around method [39] to measure the RW speeds. In the case of homogeneous uniaxial initial stress $\sigma_1(\sigma_3 = 0)$, Eq. 19.70 becomes

$$\frac{\Delta V_1}{V_0} = \left[\frac{\alpha_1 - \nu_0 \alpha_2}{2\rho_a V_0^2} + \frac{\mu}{2(\lambda + \mu)} \right] \varepsilon_{11} = A_{\|} \sigma_1 \tag{19.71}$$

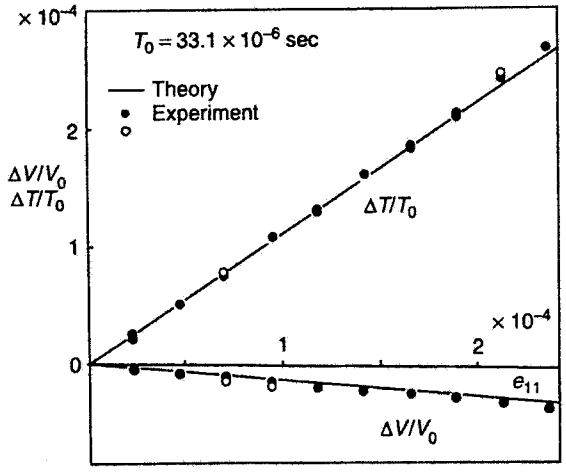

Fig. 19.6. Relative variations of Rayleigh wave transit time T and velocity V versus the uniaxial tensile strain. The strain e_{11} in the figure corresponds to $\varepsilon_{11}(\mathbf{X};\mathbf{a})$ in the text (from Hirao *et al.* [60]).

$$A_{\parallel} = \frac{1}{2}\left(\frac{\alpha_1 - \nu_0\alpha_2}{\rho_a V_0^2 E_0} + \frac{1}{3\lambda + 2\mu}\right) \tag{19.72}$$

where $A_{\parallel}$ is called the SAW acoustoelastic constant parallel to the loading direction, and E_0 and ν_0 are the Young's modulus and Poisson's ratio in the natural state, respectively. Recalling that the specimen acts as a transversely isotropic medium about the X_1 direction, one obtains in a similar way $\Delta V_3/V_0$, a change in RW speed in the X_3 direction, by replacing in Eq. 19.68 C_{11} by $C_{22} = C_{33}$, C_{12} by C_{23}, and C_{66} by $C_{44} = (C_{22} - C_{23})/2$ and by setting $\sigma_1 = 0$. $\Delta V_3/V_0$ is expressed as

$$\Delta V_3/V_0 = (V_3 - V_0)/V_0 = A_{\perp}\sigma_1 \tag{19.73}$$

where $A_{\perp}$ is called the SAW acoustoelastic constant normal to the loading direction and can be written in terms of the SOEC and TOEC. Using the SOEC and TOEC data and $\nu_0 = 0.284$ measured with a mild steel specimen under uniaxial stress σ_1, Hirao *et al.* [60] obtained an expression $\Delta V_1/V_0 = -0.31\varepsilon_{11} - 0.69\varepsilon_{22} = -0.11\varepsilon_{11}$. This is plotted in Figure 19.6 and is found in good agreement with observed variations of RW speed with strain e_{11}. (In Fig. 19.6, the strain e_{11} is actually the same as ε_{11}.) Hirao *et al.* [60] also considered the case of RW propagation along an inhomogeneous surface layer. In the latter case the RW becomes dispersive and the RW whose speed depends on frequency. The RW propagation along the inhomogeneous surface layer was also investigated by Husson [61] by a perturbation method.

Iwashimizu and Kobori [56] investigated a SAW propagating in a general direction away from the principal stress directions of a homogeneously deformed half-space material, which is isotropic in the natural state **a**. In this case the SAW no longer behaves as a RW mode and its polarization vector has a horizontal component normal to the sagittal plane defined by the propagation direction and the normal to the traction-free surface. A similar investigation on SAW propagation was extended to a slightly orthotropic half-space in the natural state by Delsanto and Clark, Jr. [62], who used a perturbation method. Barnett, Lothe, and their coworkers [63, 64] extended Stroh formalism [65] and developed the integral formalism for the solution of SAW problems. The integral formalism of Barnett *et al.* was used by Mase and Johnson [66] to study theoretically the SAW propagating on the prestressed surface of an anisotropic material.

One remarkable consequence of Iwashimizu and Kobori's investigation is that under the plane biaxial surface stresses $\sigma_{11}(\mathbf{X})$, $\sigma_{13}(\mathbf{X})$, and $\sigma_{33}(\mathbf{X})$, the phase velocity of a SAW propagating along the direction X_1 at an angle θ to the direction of principal stress σ_1 (the other principal stress being σ_3) is independent of the shear stress (or strain) and its variation with stress can be expressed as as

$$\Delta V_1/V_0 = A_{\parallel}\sigma_{11} + A_{\perp}\sigma_{33} \tag{19.74}$$

Likewise, one obtains for the SAW propagating in the X_3 direction

$$\Delta V_3/V_0 = A_{\parallel}\sigma_{33} + A_{\perp}\sigma_{11} \tag{19.75}$$

The sum and difference in Eqs. 19.74 and 19.75 are written as

$$(V_1 + V_3)/V_0 = 2 + A_S(\sigma_{11} + \sigma_{33}) \tag{19.76}$$

$$(V_1 - V_3)/V_0 = A_d(\sigma_{11} - \sigma_{33}) \tag{19.77}$$

where $A_S = A_{\parallel} + A_{\perp}$ and $A_d = A_{\parallel} - A_{\perp}$. Since $\sigma_{11} + \sigma_{33}$ is rotation-invariant, $V_1 + V_3$ is independent of a rotation of coordinates. Eq. 19.77 can be considered a SAW birefringence formula.

Two SAW acoustoelastic constants, $A_{\parallel}$ and $A_{\perp}$, are determined in a uniaxial calibration test by measuring the RW speed changes in the directions parallel and normal to

the loading direction. Then both σ_{11} and σ_{33} are calculated via Eqs. 19.74 and 19.75 from ΔV_1 and ΔV_3 measurements. The principal stress direction θ is found where the variations of the SAW speeds show symmetry about the direction. Then the shear stress σ_{13} is calculated from

$$\sigma_{13} = (1/2)(\sigma_{11} - \sigma_{33}) \tan 2\theta \tag{19.78}$$

Accurate measurements of SAW speeds were facilitated with advances in scanning acoustic microscopy (SAM) [67–69], and the SAM technique was adopted by Lee *et al.* [70] and Okade and Kawashima [71] to measure variations of SAW speeds for the determination of residual stresses. In a line-focus beam SAM [69] using water as a coupling medium, the SAW velocity $V(\theta)$ is calculated from the spacing Δz of the periodic dips of the transducer output voltage versus defocusing distance z via the equation

$$V(\theta) = \frac{V_w}{\sqrt{1 - [1 - V_w/(2f\Delta z)]^2}} \tag{19.79}$$

where V_w is the sound speed in water and f denotes the carrier frequency of ultrasonic tone bursts.

Figure 19.7 [70] shows the variations of measured leaky RW speeds parallel and normal to the loading direction X_1 with strain ϵ_{11}. They are obtained with an aluminum 6061-T6 specimen, using the line-focus beam SAM. The acoustoelastic constants $A_{\parallel}$ and $A_{\perp}$, found by curve-fitting these data into Eqs. 19.74 and 19.75, are -0.019 $(\text{GPa})^{-1}$ and 0.007 $(\text{GPa})^{-1}$.

As in the case of the bulk waves, the acoustoelastic effect on SAW speed below the elastic limit of a material that is nearly isotropic in the natural state is so small that the SAW is almost sagittally polarized, with a small horizontal component being the order of the initial strain $\epsilon_{ij}(\mathbf{X};\mathbf{a})$ relative to the sagittal component, which is unity. The opposite case arises in which a horizontal component of the SAW polarization is dominant against a sagittal component for some anisotropic crystals in a range of propagation directions on the free surface [59] and the SAW is almost shear-horizontally (SH) polarized. It is observed that in an isolated range of directions, called

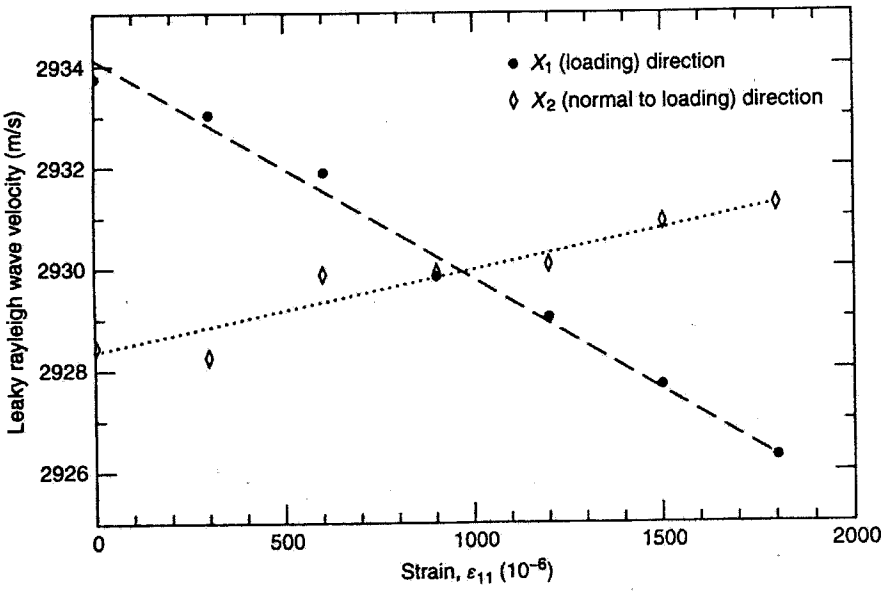

Fig. 19.7. Variation of the leaky Rayleigh wave velocities of an aluminum 6061-T6 specimen in the uniaxial tensile loading test. A dashed line is a linear curve-fit. (from Lee *et al.* [70]).

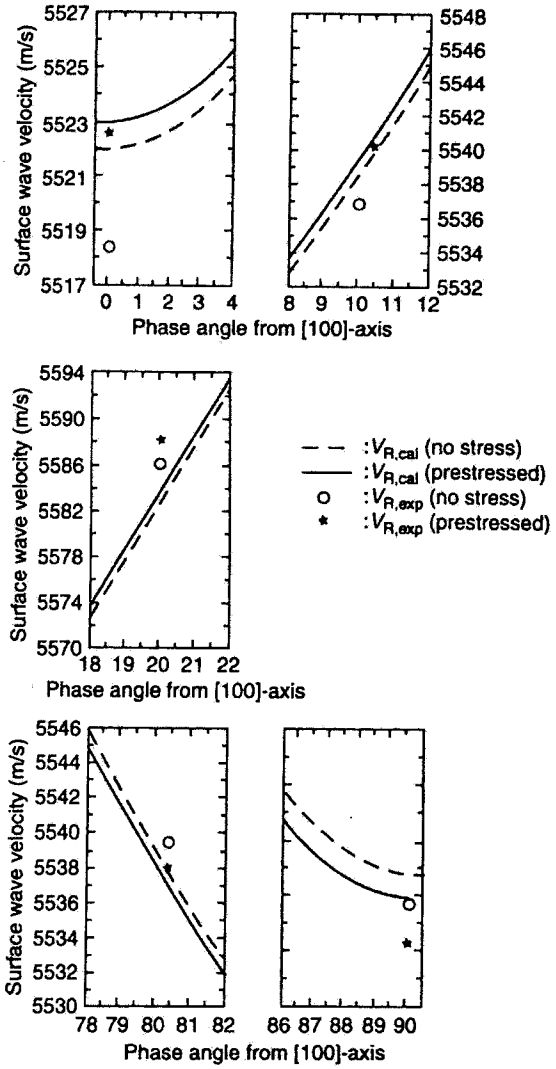

Fig. 19.8. Comparison of SAW phase velocities on the (001) surface of a MgO crystal in the natural and compressed ($\sigma_{11} = -100$ MPa) states (from Chai and Wu [74]).

the pseudo-branch on some anisotropic surfaces, pseudo-SAWs propagate whose propagation vector tilts down from the surface in the sagittal plane and which carry energy away from the surface into the interior [59,72]. The velocities of the pseudo-SAWs lie between those of slow and fast transverse bulk modes. One notable example is a copper cubic crystal, the (001) and (111) surfaces of which have the pseudo-branch. The nearly SH-polarized SAWs are unobservable by the fluid-coupled surface SAM, but the pseudo-SAWs can easily be detected by the SAM [73]. Figure 19.8 shows Chai and Wu's measurements [74] of the SAW phase velocities along 0°, 10°, 20°, 80°, and 90° directions from the [100] axis on the prestressed (001) surface of a MgO crystal by the line-focus SAM. The MgO crystal was compressed at 100 MPa along the [100] direction. The measured SAW velocities are in good agreement with those calculated from the integral formalism of Barnett *et al.* [63, 64]. Note that the SAW velocities increase near the [100] axis and decrease near the [010] axis. Between 30° and 60° directions from the [100] axis, which straddle the [110] direction at 45°, the

SAWs in the MgO crystal are nearly SH-polarized and cannot be detected by the fluid-coupled SAM. In this angular range of SH-polarized SAWs, which almost coincides with the pseudo-branch, Kim and Achenbach [73] instead measured the phase velocities of sagittally polarized pseudo-SAWs by the line-focus SAM, using the (001)-oriented stress-free Si and MgO crystals. For crystals exhibiting a substantial anisotropy, propagation and polarization behaviors are expected to be dominated by the anisotropy of the SOEC, and the acoustoelastic effect on them is of the order of the initial strain.

19.7. CONCLUSIONS

The strength of a solid under stress is characterized by the effective elastic coefficients K_{ijkl}, which in general vary nonlinearly with stress. The K_{ijkl} coefficients lack the full symmetry found in the thermodynamic elastic coefficients C_{ijkl}. $K_{ijkl} = K_{jikl}$, $K_{ijkl} = K_{ijlk}$, but $K_{ijkl} \neq K_{klij}$. K_{ijkl} and K_{klij} are related by Huang's conditions as specified in Eqs. 19.20 and 19.33. The wave propagation coefficients $\tilde{C}^S_{ijkl}$ defined in Eq. 19.31 satisfy the same symmetry relations found in the K_{ijkl} coefficients, including the same Huang's conditions. Both $[K_{\alpha\beta}]$ and $[C_{\alpha\beta}]$ $(\alpha, \beta = 1, 2, \ldots 6)$ matrices have in general 26 independent elements. The isothermal $K^T_{\alpha\beta}$ coefficients are obtained in quasi-static tension, compression, and torsion tests. The adiabatic $K^S_{\alpha\beta}$ coefficients are linearly related to the $\tilde{C}^S_{\alpha\beta}$ coefficients, and they can be determined from measurements of the phase velocities of sound waves propagating along various directions in a stressed solid medium. Huang's conditions applied to two transverse sound waves propagating in the principal directions of an orthotropic medium lead to the acoustic birefringence phenomena expressed by Eq. 19.46. These birefringence formulas can be applied to characterize residual stresses locked in structures.

The K_{ijkl} coefficients are valuable for studying the strength of solids, phase transitions, equations of state of solids, etc., at high pressures. K_{ijkl} coefficients in the initial state can be written in terms of the SOEC, TOEC, and initial strain via Eqs. 19.21, 19.15, and 19.17. The K_{ijkl} coefficients can be used to extract information on the TOEC and HOEC, which are useful for the investigation of anharmonic properties of solids.

A SAW propagating on the traction-free surface of an initially stressed semi-infinite solid modifies the shape of the surface. This results in the peculiar surface boundary conditions specified by Eq. 19.65. For a SAW propagating in the principal stress direction of an orthotropic medium, one obtains an analytical expression, such as Eq. 19.68, which relates the SAW phase velocity to the principal stress in the propagation direction and the thermodynamic elastic coefficients. For a SAW propagating in a general direction on the surface of a stressed orthotropic medium, which is isotropic in the natural state, acoustoelastic formulas similar to the case of bulk waves are found. These are given by Eqs. 19.74–19.77. A notable feature in these equations is that they are independent of the shear stress or shear strain on the surface. These acoustoelastic formulas can be used to determine biaxial surface stresses.

ACKNOWLEDGMENT

The authors greatly appreciate the financial support from the Physics Program of the Office of Naval Research.

References

1. Voigt, W. (1928). *Lehrbuch der Kristallphysik*, Berlin: Teubner.
2. Kim, K.Y. (1996). *Phys. Rev.* **B 54**: 6245.

3. Murnaghan, F.D. (1951). *Finite Deformation of an Elastic Solid*, New York: Wiley.
4. Born, M. and Huang, K. (1954). *Dynamical Theory of Crystal Lattices*, Oxford: Clarendon.
5. Leibfried, G. and Ludwig, W. (1961). In *Solid State Physics-Advances in Research and Applications*, Ehrenreich, H., Seitz, F., and Turnbull, D., eds., pp. 275–444, vol. 12, New York: Academic.
6. Maradudin, A.A., Montroll, E.W., Weiss, G.H., and Ipatova, I.P. (1971). *Theory of Lattice Dynamics in the Harmonic Approximation*, Supplement 3, 2nd ed., New York: Academic.
7. Brugger, K. (1964). *Phys. Rev.* **133**: A1611.
8. Thurston, R.N. (1965). *J. Acoust. Soc. Am.* **37**: 348.
9. Birch, F. (1947). *Phys. Rev.* **71**: 809.
10. Toupin, R.A. and Bernstein, B. (1961). *J. Acoust. Soc. Am.* **33**: 216.
11. Thurston, R.N. and Brugger, K. (1964). *Phys. Rev.* **A 133**: 1604.
12. Wallace, D.C. (1970). In *Solid State Physics: Advances in Research and Applications*, Ehrenreich, H., Seitz, F., and Turnbull, D., eds., pp. 301–404, vol. 25, New York: Academic.
13. Hughes, D.S. and Kelly, J.L. (1953). *Phys. Rev.* **92**: 1145.
14. Bateman, T.B., Mason, W.P., and McSkimin, H.J. (1961). *J. Appl. Phys.* **32**: 928.
15. Seeger, A. and Buck, O. (1960). *Z. Naturforsch* **15a**: 1056.
16. Every, A.G. and McCurdy, A.K. (1992). In *Numerical Data and Functional Relationships in Science and Technology*, Landolt-Bornstein, New Series, Group III, Vol. 29a, Hellwege, K.-H. and Hellwege, A.M., eds., Berlin: Springer-Verlag.
17. Garland, C.W. (1970). In *Physical Acoustics*, pp. 51–148, vol. 12, Mason, W.P. and Thurston, R.N., eds., New York: Academic.
18. Huang, K. (1950). *Proc. R. Soc. London, Ser. A* **203**: 178.
19. Tokuoka, T. and Iwashimizu, Y. (1968). *Int. J. Solids Structures* **4**: 383.
20. Tokuoka, T. and Saito, M. (1969). *J. Acoust. Soc. Am.* **45**: 1241.
21. Iwashimizu, Y. and Kubomura, K. (1973). *Int. J. Solids Structures* **9**: 99.
22. King, R.B. and Fortunko, C.M. (1983). *J. Appl. Phys.* **54**: 3027.
23. Kim, K.Y. and Sachse, W. (1996). *J. Appl. Phys.* **80**: 4934.
24. Kim, K.Y., Wu, T.-T., and Sachse, W. (1997). *J. Acoust. Soc. Am.* **102**: 3333.
25. Pao, Y.-H., Sachse, W., and Fukuoka, H. (1984). In *Physical Acoustics*, pp. 61–143, vol. 17, Mason, W.P. and Thurston, R.N., eds., New York: Academic.
26. Pao, Y.-H. and Gamer, U. (1985). *J. Acoust. Soc. Am.* **77**: 806.
27. Lazarus, D. (1949). *Phys. Rev.* **76**: 545.
28. Barsch, G.R. and Chang, Z.P. (1969). *Phys. Stat. Sol.* **19**: 139.
29. Macdonald, J.R. (1969). *Rev. Mod. Phys.* **41**: 316.
30. Birch, F. (1952). *J. Geophys. Res.* **57**: 227.
31. Cook, R.K. (1957). *J. Acoust. Soc. Am.* **29**: 445.
32. Thurston, R.N. (1967). *J. Acoust. Soc. Am.* **41**: 1093.
33. Kim, K.Y. and Sachse, W. (2000). *J. Mater. Sci.* **35**(13).
34. Ruoff, A.L., Xia, H., and Xia, Q. (1992). *Rev. Sci. Instrum.* **63**: 4342.
35. Williams, J. and Lamb, J. (1958). *J. Acoust. Soc. Am.* **30**: 308.
36. McSkimin, H.J. (1961). *J. Acoust. Soc. Am.* **33**: 12.
37. McSkimin, H.J. (1962). *J. Acoust. Soc. Am.* **34**: 609.
38. Papadakis, E.P. (1976). In *Physical Acoustics*, pp. 277–374, vol. 12, Mason, W.P. and Thurston, R.N., eds., New York: Academic.
39. Forgacs, R.L. (1960). *IRE Trans. Instrum.* **I-9**: 359.
40. Bolef, D.I. and Miller, J.G. (1971). In *Physical Acoustics*, pp. 95–201, vol. 8, Mason, W.P. and Thurston, R.N., eds., New York: Academic.
41. Miller, J.G. and Bolef, D.I. (1969). *Rev. Sci. Instrum.* **40**: 915.
42. Petersen, G., Chcik, B.B., Fortunko, C.M., and Hirao, M. (1973). *Rev. Sci. Instrum.* **65**: 192.
43. Dobbs, E.R. (1973). In *Physical Acoustics*, pp. 127–191, vol. 10, Mason, W.P. and Thurston, R.N., eds., New York: Academic.
44. Fleury, P.A. (1970). In *Physical Acoustics*, pp. 1–64, vol. 6, Mason, W.P. and Thruston, R.N., eds., New York: Academic.
45. Egle, D.M. and Bray, D.E. (1976). *J. Acoust. Soc. Am.* **60**: 741.
46. Hsu, N.N. (1974). *Exp. Mech.* **14**: 169.
47. Okada, K. (1981). *Exp. Mech.* **21**: 461.
48. Man, C.-S. and Lu, W.Y. (1987). *J. Elasticity* **17**: 159.
49. Pao, Y.-H., Wu, T.-T., and Gamer, U. (1991). *J. Appl. Mech.* **58**: 11.
50. Wu, T.-T., Hirao, M., and Pao, Y.-H. (1991). *J. Appl. Mech.* **58**: 18.
51. Katahara, K.W., Nimalendran, M., Manghnani, M.H., and Fisher, E.S. (1979). *J. Phys. F: Metal Phys.* **9**: 2167.
52. Polian, A., Besson, J.M., Grimsditch, M., and Grosshans, W.A. (1989). *Phys. Rev.* **B 39**: 1332.
53. Ruoff, A.L., Lincoln, R.C., and Chen, Y.C. (1973). *J. Phys.* **D 6**: 1295.
54. Degtyar, A.D. and Rokhlin, S.I. (1995). *J. Appl. Phys.* **78**: 1547.

55. Hayes, M. and Rivlin, R.S. (1961). *Arch. Rational. Mech. Anal.* **8**: 358.
56. Iwashimizu, Y. and Kobori, O. (1978). *J. Acoust. Soc. Am.* **64**: 910.
57. Stoneley, R. (1963). *Geophys. J.* **8**: 176.
58. Royer, D. and Dieulesaint, E. (1984). *J. Acoust. Soc. Am.* **76**: 1438.
59. Farnell, G.W. (1970). In *Physical Acoustics*, pp. 109–166, vol. 6, Mason, W.P. and Thurston, R.N., eds., New York: Academic.
60. Hirao, M., Fukuoka, H., and Hori, K. (1981). *J. Appl. Mech.* **48**: 119.
61. Husson, D. (1985). *J. Appl. Phys.* **57**: 1562.
62. Delsanto, P.P., and Clark, Jr., A.V. (1987). *J. Acoust. Soc. Am.* **81**: 952.
63. Barnett, D.M., Lothe, J., Nishioka, K., and Asaro, R.J. (1973). *J. Phys. F: Metal Phys.* **3**: 1083.
64. Barnett, D.M., Nishioka, K., and Lothe, J. (1973). *Phys. Stat. Sol.* **B 55**: K115.
65. Stroh, A.N. (1962). *J. Math. Phys.* **41**: 77.
66. Mase, G.T. and Johnson, G.C. (1987). *J. Appl. Mech.* **54**: 127.
67. Lemons, R.A. and Quate, C.F. (1974). *Appl. Phys. Lett.* **25**: 251.
68. Briggs, A. (1992). *Acoustic Microscopy*, Oxford: Clarendow.
69. Kushibiki, J. and Chubashi, N. (1985). *IEEE Trans. Sonics Ultrason.* **SU-32**: 189.
70. Lee, Y.-C., Kim, J.O., and Achenbach, J.D. (1994). *Ultrasonics* **32**: 359.
71. Okade, M. and Kawashima, K. (1998). *Ultrasonics* **36**: 933.
72. Rollins, Jr., F.R., Lim, T.C., and Farnell, G.W. (1968). *Appl. Phys. Lett.* **12**: 236.
73. Kim, J.O. and Achenbach, J.D. (1992). *Thin Solid Films* **214**: 25.
74. Chai, J.-F. and Wu, T.-T. (1996). *NDT & E Int.* **29**: 281.